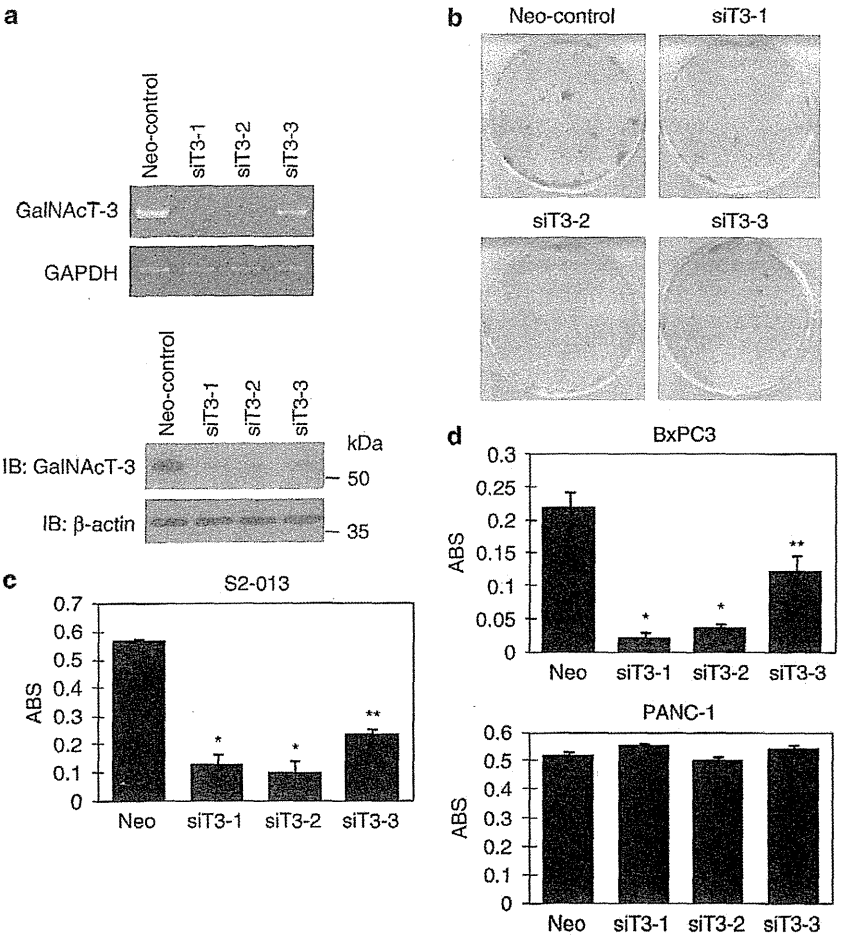

Figure 2 The growth-inhibitory effect of GalNAc-T3 siRNAs in PDAC cells. (**a**) Three GalNAc-T3 siRNA expression vectors (siT3-1, siT3-2 and siT3-3) and a Neo-pSUPERgfp vector as a negative control were transiently transfected into S2-013 cells. The knockdown effect of GalNAc-T3 was validated by RT–PCR (upper panels) and western blotting using an anti-GalNAc-T3 antibody (lower panels). (**b**) Colony formation assays of S2-013 cells were performed 14 days after neomycin selection. The data are representative of three independent experiments. (**c**) MTT assays of S2-013 cells were performed to evaluate cell viability at 14 days with neomycin selection. The data are representative of three independent experiments and are shown as the means ± s.e.m. $*P<0.001$ and $**P<0.005$ compared with control cells. (**d**) MTT assays of BxPC3 and PANC-1 cells were performed to evaluate cell viability at 14 days with neomycin selection. The data are representative of three independent experiments and are shown as the means ± s.e.m. $*P<0.001$ and $**P<0.005$ compared with control cells. GalNAc-T, UDP-GalNAc:polypeptide *N*-acetylgalactosaminyl-transferase; MTT, 3-(4,5-dimethylthiazol-2-yl)-2,5-diphenyltetrazolium bromide; PDAC, pancreatic ductal adenocarcinoma; RT–PCR, reverse transcription–PCR; siRNA, small interfering RNA.

variable glycoforms (Kondo *et al.*, 2006). Two 40-kDa bands were identified in GalNAc-T3 RNAi S2-013 cells, whereas only one band was observed in the control cells (Figure 6a). The 40-kDa bands were excised and analyzed by using a Q-TOF Ultima tandem mass spectrometer (Q-TOF-MS) after in-gel trypsin digestion and identified as GNAT1. The peptide sequence coverage was 13% (Figure 6b). GNAT1 is a membrane-associated, three-subunit, guanine nucleotide-binding protein (G-protein), which stimulates the coupling of rhodopsin and cGMP-phoshodiesterase during visual impulses (Ruiz-Avila *et al.*, 1995). The function of GNAT1 in PDAC cells is currently unknown. Two bands of GNAT1 (40-kDa-1 and 40-kDa-2) were confirmed in the membrane fractions from GalNAc-T3 RNAi S2-013 cells by western blotting (Figure 7a). Only one band was observed in the control S2-013 cells (40-kDa-2; Figure 7a). Additionally, both the 40-kDa GNAT1 bands were more abundantly expressed in the cytoplasmic fractions of GalNAc-T3 RNAi S2-013 cells as compared with that in the control cells (Figure 7b). In immunocytochemical staining, GNAT1 was observed in the cytoplasm and the membrane of GalNAc-T3 RNAi S2-013 cells, whereas GNAT1 was expressed at the cell membrane, and only a little expression of GNAT1 was seen in the cytoplasm of the control cells (Figure 7c). Thus, suppression of GalNAc-T3 produced a different form of GNAT1 (40-kDa-1) and changed its intracellular distribution. To test whether GalNAc-T3 affects the stability of the GNAT1 protein, we analyzed the expression levels of GNAT1 mRNA and protein in total lysates of control S2-013 and GalNAc-T3 RNAi

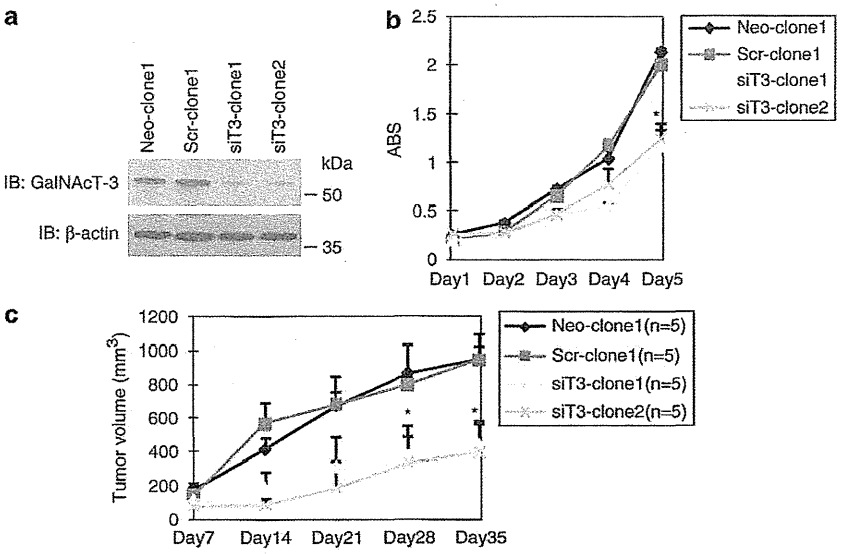

Figure 3 Stable knockdown of GalNAc-T3 suppresses the cell growth of PDAC. (**a**) Western blotting using anti-GalNAc-T3 antibody showing two S2-013 (siT3-clone1 and siT3-clone2) clones transfected with siRNA for GalNAc-T3 and compared to mock (Neo-1) and scrambled (Scr-1) control clones. (**b**) MTT assays in stable control and GalNAc-T3 RNAi S2-013 cells. The data are representative of three independent experiments and are shown as the means ± s.e.m. $*P<0.001$ compared with the control cells. (**c**) Tumor xenografts in stable control and GalNAc-T3 RNAi S2-013 cells. Two control and GalNAc-T3 RNAi clones were incubated in the dorsa at the proximal midline of 7-week-old nude mice; $n=5$. The error bars indicate the s.e.m. $*P<0.005$ compared with control cells. GalNAc-T, UDP-GalNAc:polypeptide *N*-acetylgalactosaminyl-transferase; MTT, 3-(4,5-dimethylthiazol-2-yl)-2,5-diphenyltetrazolium bromide; PDAC, pancreatic ductal adenocarcinoma; RNAi, RNA interference; siRNA, small interfering RNA.

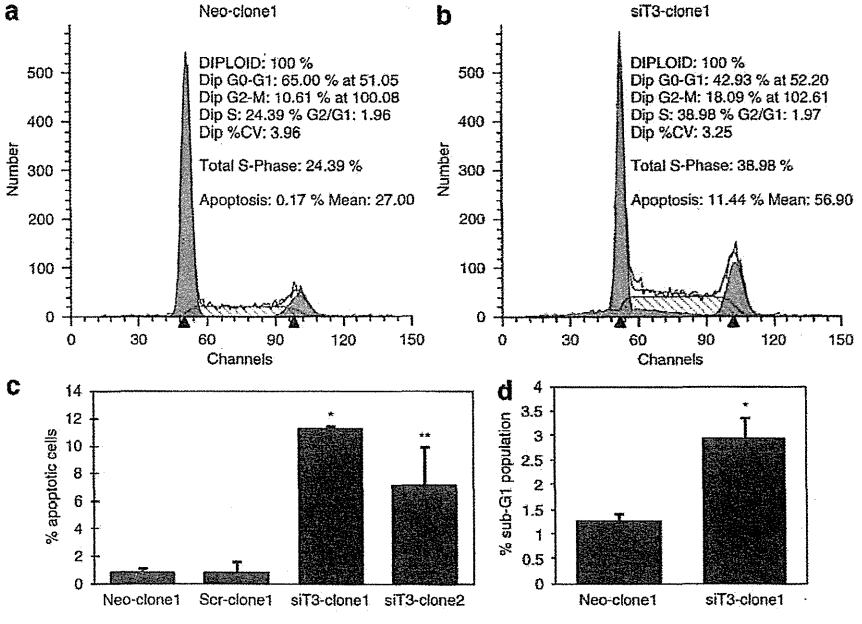

Figure 4 Flow cytometric analysis of cell-cycle distribution and apoptosis in stable control and GalNAc-T3 RNAi S2-013 cells. (**a**, **b**) Cells were grown to approximately 70% confluence and removed from culture surfaces by trypsinization, and DNA content and apoptosis were determined. Raw data were modeled using the ModFit cell-cycle analysis software. The profiles are representative histograms of triplicate assays. (**a**) Control. (**b**) GalNAc-T3 RNAi cells. (**c**) The percentage of apoptotic cells is shown between the control and GalNAc-T3 RNAi S2-013 cells. The experiments were repeated three times. $*P<0.001$ and $**P<0.005$ compared with the control cells. (**d**) The percentage of cells in the sub-G_1 population was determined from at least 10 000 ungated cells between the control and the GalNAc-T3 RNAi S2-013 cells. The experiments were repeated three times. $*P<0.05$ compared with the control cells. GalNAc-T, UDP-GalNAc:polypeptide *N*-acetylgalactosaminyl-transferase; RNAi, RNA interference.

cells. We found no differences in the expression of GNAT1 mRNA between the control and the GalNAc-T3 RNAi S2-013 cells (Figure 7d); however, the steady-state level of 40-kDa-2, which is expressed in control cells, was decreased and the altered 40-kDa-1 form was produced after GalNAc-T3 knockdown (Figure 7e). It is

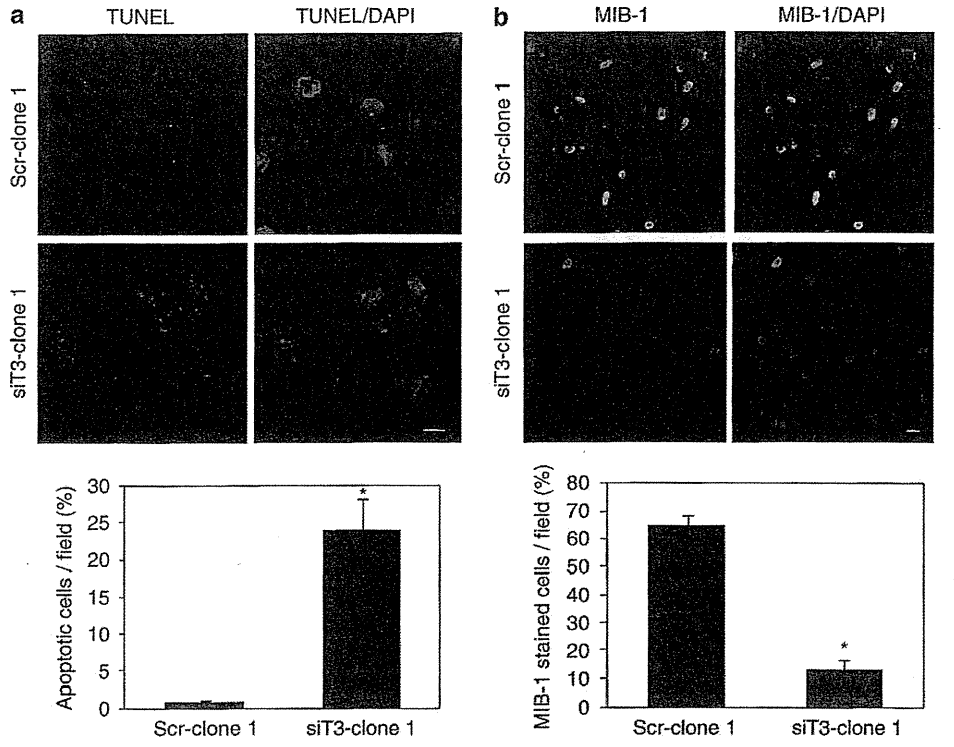

Figure 5 The effects of GalNAc-T3 on cell growth and survival. (**a**) Control and GalNAc-T3 RNAi S2-013 cells were subjected to *in situ* apoptosis detection assay. The red signal indicates apoptosis. Blue: DAPI staining. The number of apoptotic cells was counted. Cells in four defined areas per group per experiment were quantified. The data are representative of three independent experiments. The columns indicate the mean and the bars indicate the s.d. $*P<0.001$ compared with control cells. Bar: 10 μm. (**b**) Immunocytochemical staining in control and GalNAc-T3 RNAi S2-013 cells, as determined with an anti-MIB-1 antibody (green). Blue: DAPI staining. The percentage of MIB-1-stained cells is shown. Cells in four defined areas per group per experiment were quantified. The data are representative of three independent experiments. The columns indicate the mean and the bars indicate the s.d. $*P<0.001$ compared with control cells. Bar: 10 μm. DAPI, 4,6-diamidino-2-phenylindole; GalNAc-T, UDP-GalNAc:polypeptide *N*-acetylgalactosaminyl-transferase; RNAi, RNA interference.

possible that knocking down endogenous GalNAc-T3 decreased the stability of the 40-kDa-2 form, perhaps by carbohydrate structural changes or through loss of *O*-glycosylation, and in turn produced the 40-kDa-1 form. These results suggest that GalNAc-T3 post-translationally catalyzes GNAT1, and that GNAT1 may be a substrate protein of GalNAc-T3.

Identification of O*-glycosylation in GNAT1*

We next assessed the *O*-glycosylation status of GNAT1 in S2-013 cells. First, total lysates from S2-013 cells were treated with sialidase to determine the effects of removal of sialic acid residues from *O*-glycans or *N*-glycans in GNAT1 (Figure 8a). Mobility shifts before and after sialidase treatment showed that GNAT1 from S2-013 cells was sialidase-sensitive. This result indicates that GNAT1 is a glycoprotein that has *O*-glycans or *N*-glycans. To test whether the carbohydrates of GNAT1 were *O*-glycosylated, total S2-013 cell lysates were treated with peptide *N*-glycosidase-F to remove the *N*-linked glycans (Figure 8b). We confirmed that the band of the single-span, transmembrane *N*-glycoprotein E-cadherin was peptide *N*-glycosidase-F-sensitive and found no obvious differences in the band positions of GNAT1, thus indicating that GNAT1 is not glycosylated by *N*-linked carbohydrates. Additionally, S2-013 cell lysates were incubated with *O*-sialoglycoprotein endopeptidase (OSGE; Mellors and Lo, 1995), which cleaves the protein at *O*-linked glycans (Figure 8c). The GNAT1 band was significantly reduced after OSGE treatment. These results indicate that GNAT1 is an *O*-glycosylated glycoprotein.

We next assessed the potential *O*-glycosylation of GNAT1 in GalNAc-T3 RNAi S2-013 cells. The 40-kDa-1 form was not digested by OSGE treatment, whereas the 40-kDa-2 form was OSGE-sensitive (Figure 8d). A non-specific band was detected by western blotting using an anti-GNAT1 antibody (Figures 8a, c and d). This band was at a much lower molecular weight than the apparent molecular weight of GNAT1, was seen in cell lysates with or without enzyme treatment, and was not shifted by the treatment. Thus, these results indicate that this band is not associated with GNAT1. Subsequently, the glycochain of GNAT1 was detected by a G.P. Sensor kit as the same-sized molecule recognized by western blotting in control cells (Figure 8e). In concordance with the results shown in Figures 7e and 8d, the 40-kDa-2 form was decreased and the 40-kDa-1 form was not detected in GalNAc-T3 RNAi S2-013 cells

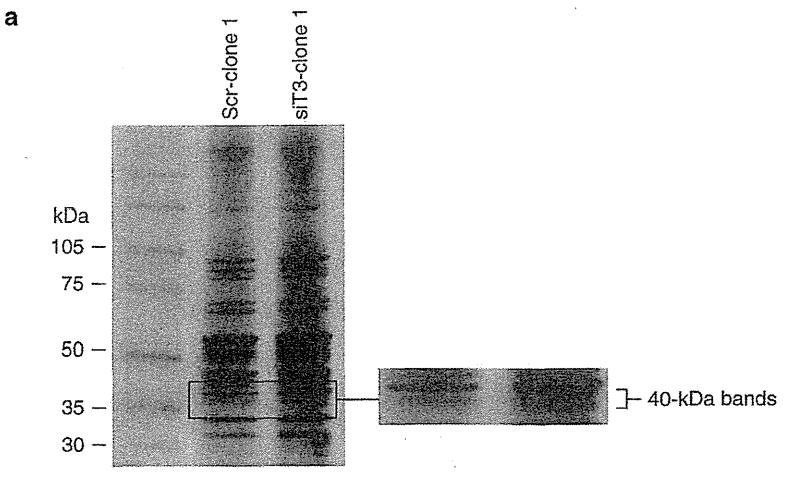

b

Protein: guanine nucleotide binding protein, alpha transducing activity polypeptide 1
Sequence Coverage: **13%**

1MGAGASAEEKHSRELEKKLKEDAEKDARTVKLLLLGAGESGKSTIVKQMKIIHQDGYSLE
61ECLEFIAIIYGNTLQSILAIVRAMTTLNIQYGDSARQDDARKLMHMADTIEEGTMPKEMS
121DIIQRLWKDSGIQACFERASEYQLNDSAGYYLSDLERLVTPGYVPTEQDVLRSRVKTTGI
181IETQFSFKDLNFRMFDVGGQRSERKKWIHCFEGVTCIIFIAALSAYDMVLVEDDEVNRMH
241ESLHLFNSICNHRYFATTSIVLFLNKKDVFFEKIKKAHLSICFPDYDGPNTYEDAGNYIK
301VQFLELNMRRDVKEIYSHMTCATDTQNVKFVFDAVTDIIIKENLKDCGLF

Figure 6 Identification of GalNAc-T3-associated proteins. (**a**) Membrane fractionated proteins from control and GalNAc-T3 RNAi S2-013 cells were examined by silver staining analysis. (**b**) Percent coverage for GNAT1 is represented by the identified peptides in the total protein sequence (accession number NM_032166). GalNAc-T, UDP-GalNAc:polypeptide *N*-acetylgalactosaminyl-transferase; GNAT1, α-transducing activity polypeptide-1; RNAi, RNA interference.

(Figure 8e). These results indicate that the 40-kDa-1 form was not *O*-glycosylated by knocking down GalNAc-T3 and that GNAT1 is a specific substrate of GalNAc-T3.

Knockdown effects of GNAT1 on the viability of PDAC cells

MTT assays were used to examine the effect of reduced GNAT1 expression on the cell growth of S2-013 cells, in which GNAT1 was highly expressed, and in GNAT1-null PANC-1 cells. As shown by western blot analysis, GNAT1 expression was markedly reduced in S2-013 cells 72 h after transfection with the GNAT1-targeting small interfering RNA (siRNA) oligonucleotide, in contrast to cells transfected with the scrambled siRNA oligonucleotide (Figure 9a). As a consequence of reduced GNAT1 expression by siRNA, a significant decrease in S2-013 cell growth was observed; however, no significant differences were observed in PANC-1 cells in which GNAT1 was not expressed (Figure 9b). Additionally, suppression of GNAT1 in S2-013 cells decreased cell growth as assessed by MIB-1 staining (Figure 9c) and increased apoptosis in *in situ* TUNEL staining (Figure 9d). These studies demonstrate an important role of GNAT1 in PDAC cell viability.

Discussion

O-glycosylated proteins are associated with the differentiation and malignant potential of cancers, such as altered cell adhesion, invasion, metastasis, recurrence and prognosis (Brockhausen, 1999). In numerous pancreatic pathological situations, *O*-glycosylated protein expression is deregulated and aberrant expression of *O*-glycosylated proteins is often associated with poor prognosis (Braga *et al.*, 1992; Reis *et al.*, 1999). *O*-glycosylation is important in many aspects of survival and protection of cells and organisms. Carcinomas commonly overexpress *O*-linked glycans in the form of cell-surface and secreted glycoproteins that present ligands for adhesion receptors, such as the selectins, which promote the ability of tumor cells to interact with host platelets, leucocytes and endothelial cells (Fuster and Esko, 2005). Thus, GalNAc-Ts that regulate the initiation of the *O*-glycosylation of glycoproteins are important for understanding aspects of tumor-associated aberrant *O*-glycosylation. We found GalNAc-T3 to be overexpressed in 66% of PDACs when compared with the normal pancreas. *O*-glycosylation occurs in part by differential expression of GalNAc-Ts in normal tissues and tumors (White *et al.*, 1995; Bennett *et al.*, 1996), suggesting that the differential expression of

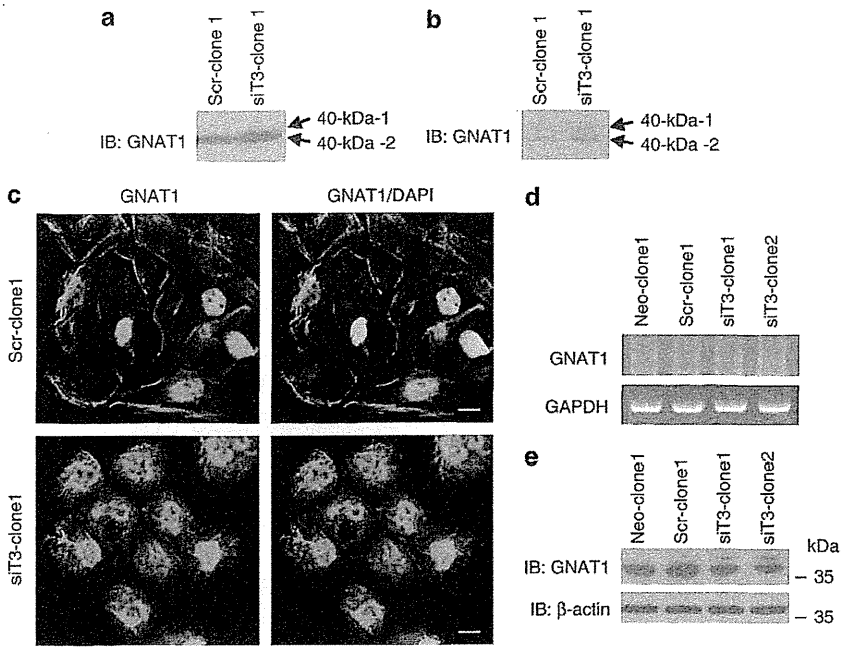

Figure 7 GNAT1 is a potential substrate for GalNAc-T3. (**a**) Membrane fractionation of control and GalNAc-T3 RNAi S2-013 cells followed by western blotting using anti-GNAT1 antibody. (**b**) Cytosolic fractionation of control and GalNAc-T3 RNAi S2-013 cells followed by western blotting using anti-GNAT1 antibody. (**c**) Immunocytochemical staining in control and GalNAc-T3 RNAi S2-013 cells, as determined by an anti-GNAT1 antibody (green) and DAPI staining (blue). Bars: 10 μm. (**d**) RT–PCR analysis of steady-state levels of GNAT1 mRNA in control and GalNAc-T3 RNAi S2-013 cells. (**e**) Western blot analysis of steady-state levels of GNAT1 protein in control and GalNAc-T3 RNAi S2-013 cells. DAPI, 4,6-diamidino-2-phenylindole; GalNAc-T, UDP-GalNAc:polypeptide *N*-acetylgalactosaminyl-transferase; GNAT1, α-transducing activity polypeptide-1; RNAi, RNA interference; RT–PCR, reverse transcription–PCR.

O-linked carbohydrate antigens such as CA19-9 and carcinoembrionic antigen in PDAC may be explained by the differential expression and the activity of specific GalNAc-Ts. Even though the extent of change in glycosylation owing to malignancy or how clustered *O*-glycosylation occurs have not been studied in detail, overexpression of GalNAc-T3 in PDAC may be associated with aberrant production of tumor-associated *O*-glycosylation.

We showed that suppression of GalNAc-T3 by RNAi significantly attenuates the cell growth/survival of PDAC cells *in vitro* and *in vivo*. These results indicate that overexpressed GalNAc-T3 in PDAC cells is capable of *O*-glycosylation in a differential manner as compared with the normal pancreatic epithelium, and that formation of uncommon structures or novel sites of glycosylation owing to aberrant glycosylation could contribute to malignant behavior. Because carbohydrates cannot be mutated directly, it is likely that GalNAc-T3 acts on substrate proteins that are important for the growth and/or survival of PDAC cells, and thereby contributes to cell growth/survival in an epigenetic manner based on the substrate specificities of these proteins. By Q-TOF analysis of control and GalNAc-T3 RNAi S2-013 cells, we identified a membrane-associated G-protein, GNAT1, as a substrate candidate for GalNAc-T3. We showed that by knocking down endogenous GNAT1, the growth/survival of PDAC cells was significantly suppressed, implying that GalNAc-T3 may function to induce cell viability through abnormal glycosylation of its substrates.

The mechanism by which knockdown of GalNAc-T3 decreases cell viability in S2-013 cells is through inhibition of proliferation and induction of apoptosis. Cell proliferation and apoptosis are linked by cell-cycle regulators and apoptotic stimuli that affect both processes (Alenzi, 2004). The phosphatidylinositide-3-OH kinase/Akt and the mitogen-activated protein kinase/extracellular signal-regulated kinase pathways have central roles in the regulation of cell proliferation and survival (Merighi *et al.*, 2006). Nuclear factor-κB promotes cell survival through expression of genes encoding antiapoptotic proteins that directly block caspase activation (Andersen *et al.*, 2005). In our study, GalNAc-T3 did not change the activity of extracellular signal-regulated kinase-1/2, Akt or nuclear factor-κB, and the signal transduction pathway involved in GalNAc-T3-stimulated PDAC cell growth/survival is still unknown.

GNAT1 is an essential G-protein in the rod phototransduction pathway and converts the light stimulation of photoreceptor opsins into the activation of cyclic GMP phosphodiesterase (Ruiz-Avila *et al.*, 1995). The post-translational modifications of GNAT1 are currently unknown. We showed that GNAT1 is an *O*-glycosylated protein (Figures 8a–c, e) and that the increased molecular size of GNAT1 (the 40-kDa-1 form) produced by GalNAc-T3 knockdown has no *O*-glycans

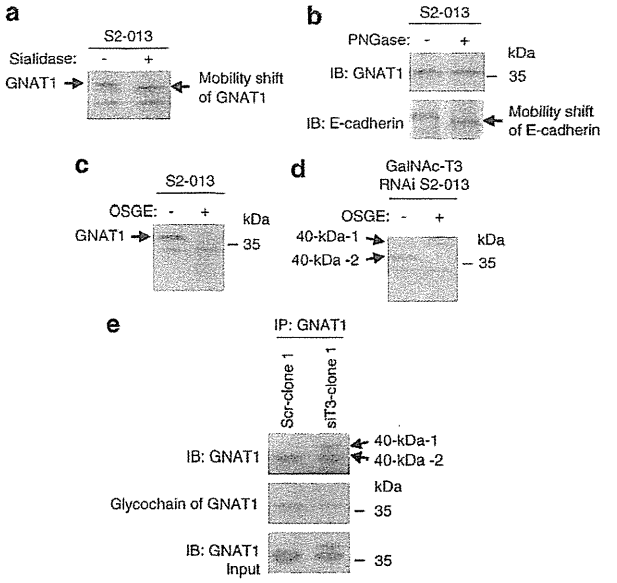

Figure 8 GNAT1 is an *O*-glycosylated protein. (**a**) Total cell lysates from S2-013 cells were treated with sialidase followed by western blotting using an anti-GNAT1 antibody. (**b**) Total cell lysates from S2-013 cells were treated with peptide *N*-glycosidase-F followed by western blotting using an anti-GNAT1 antibody and an anti-E-cadherin antibody as positive control of peptide *N*-glycosidase-F treatment. (**c**) Total cell lysates from S2-013 cells were treated with OSGE followed by western blotting using an anti-GNAT1 antibody. (**d**) Total cell lysates from GalNAc-T3 RNAi S2-013 cells (siT3-clone1) were treated with OSGE followed by western blotting using an anti-GNAT1 antibody. (**e**) Western blotting of immunoprecipitated GNAT1 from control and GalNAc-T3 RNAi S2-013 cells using an anti-GNAT1 antibody and detection of glycochains of GNAT1. GalNAc-T, UDP-GalNAc:polypeptide *N*-acetylgalactosaminyl-transferase; GNAT1, α-transducing activity polypeptide-1; OSGE, *O*-sialoglycoprotein endopeptidase; RNAi, RNA interference.

(Figures 8d and e). This indicates that GalNAc-T3 is associated with the cancer-associated *O*-glycosylation of GNAT1. We noted that GNAT1 in control S2-013 cells remains bound to membranes (Figures 7a and c) and knocking down GalNAc-T3 changed the subcellular distribution of GNAT1 from the plasma membrane to the cytoplasm (Figures 7b and c). It is possible that the 40-kDa-1 form of GNAT1 produced by GalNAc-T3 knockdown is predominantly expressed in the cytoplasm owing to loss of *O*-glycosyl structures. When rod GNAT1 is stimulated by light, its subunits dissociate, leave the membrane and equilibrate throughout the rod cell (Rosenzweig *et al.*, 2007). The cone transducin subunits do not dissociate during activation and remain sequestered within the membranes, indicating that the subunits of GNAT1 remain associated during activation in their native environments (Rosenzweig *et al.*, 2007). Our results suggest a new and unique finding in PDAC cells, that the altered structure of the *O*-glycans of GNAT1 could reflect its membrane affinity and intracellular distribution.

It has been known that malignant transformation is associated with abnormal glycosylation, resulting in the expression of altered carbohydrate determinants (Kannagi *et al.*, 2004). Knockdown of either GalNAc-T3 or GNAT1 significantly attenuated the growth and survival of PDAC cells, and thus it is likely that the 40-kDa-2 form of GNAT1 is associated with cell viability; however, the 40-kDa-1 form produced by GalNAc-T3 knockdown does not function to increase cell growth/survival. The underexpression, truncation or altered branching patterns of certain glycans correlate with cell growth (Fuster and Esko, 2005). Altered *O*-glycans expressing terminal galactose in pancreatic and colon cancers suppress apoptosis, possibly through binding to a member of the β-galactoside-binding proteins, galectin-3 (Takenaka *et al.*, 2004). Other studies have shown that upregulated biosynthesis of complex *O*-glycosidically linked glycans and galectin-3 favor breast cancer progression and brain metastasis (Mayoral *et al.*, 2008; Li *et al.*, 2010). Thus, a change in the *O*-glycosylation of GNAT1 could contribute to a change toward a cancer phenotype and to a malignant behavior. Future studies are essential for determining the structure and sites of *O*-glycans in GNAT1, by using MS to analyze the *O*-glycans released from GNAT1 by OSGE digestion. Furthermore, the differences between the 40-kDa-1 and 40-kDa-2 forms should be determined in order to evaluate whether structural changes occur as a result of alterations in the expression levels of GalNAc-T3. Thus, further studies are needed to identify the substrate *O*-glycosylated proteins of GalNAc-T3 that are essential for the cell growth and/or survival of PDAC cells. Given the broad spectrum of the *O*-glycoforms that are catalyzed by GalNAc-T3 on substrate proteins, these proteins should be promising targets for the development of novel drugs for PDAC patients.

Materials and methods

Cell culture

The human PDAC cell lines PANC-1, BxPC3, SUIT-2, COLO357, HPAF and MIA-PaCa2 were purchased from the American Type Culture Collection (ATCC). The human PDAC cell line S2-013, which is a sub-line of SUIT-2, was obtained from Dr T Iwamura (Iwamura *et al.*, 1987). HPNE immortalized normal pancreatic epithelial cells were a gift from Dr Ouellette (Lee *et al.*, 2005). Cells were grown in Dulbecco's modified Eagle's medium (Gibco-BRL, Carlsbad, CA, USA) supplemented with 10% heat-inactivated fetal calf serum at 37 °C in a humidified atmosphere saturated with 5% CO_2.

Antibodies

Polyclonal antibodies against human GalNAc-T3 were generated by multiple immunizations of a New Zealand white rabbit using synthetic peptides as described previously (Nomoto *et al.*, 1999). The rabbit anti-GNAT1 antibody (ab3504) was purchased from Abcam (Cambridge, MA, USA). A chicken Alexa-488-conjugated anti-rabbit IgG secondary antibody was obtained from Molecular Probes (Carlsbad, CA, USA).

Generation of stable knockdown cell lines of GalNAc-T3

We used a pSUPERgfp vector (OligoEngine, Seattle, WA, USA) for expression of siRNA. The target sequences for the

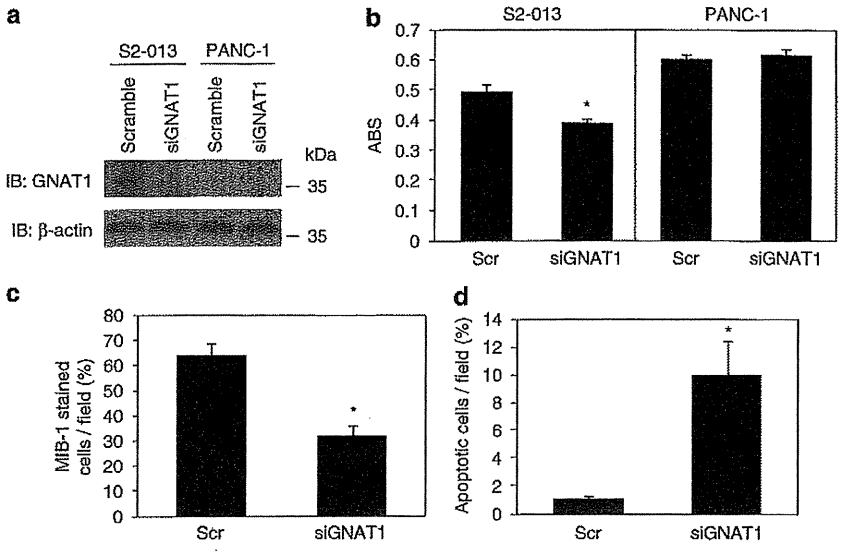

Figure 9 GNAT1 induces the cell growth and survival of PDAC cells. (**a**) siRNA oligonucleotides targeting GNAT1 (siGNAT1) and negative scrambled control (Scr) were transiently transfected into S2-013 and PANC-1 cells. Western blotting validated the knockdown effect of GNAT1 in S2-013 cells. (**b**) MTT assays of S2-013 and PANC-1 cells were performed to evaluate cell viability. The data are representative of three independent experiments and are shown as the means ± s.e.m. $^*P<0.005$ compared with scrambled control cells. (**c**) siRNA oligonucleotides targeting GNAT1 and negative scrambled control were transiently transfected into S2-013 cells. The percentage of MIB-1-stained cells is shown. Cells in four defined areas per group per experiment were quantified. The data are representative of three independent experiments. The columns indicate the mean and the bars indicate the s.d. $^*P<0.005$ compared with control cells. (**d**) Control and GNAT1 RNAi S2-013 cells were subjected to *in situ* apoptosis detection assay. Cells in four defined areas per group per experiment were quantified. The data are representative of three independent experiments. The columns indicate the mean and the bars indicate the s.d. $^*P<0.005$ compared with control cells. GNAT1, α-transducing activity polypeptide-1; MTT, 3-(4,5-dimethylthiazol-2-yl)-2,5-diphenyltetrazolium bromide; PDAC, pancreatic ductal adenocarcinoma; RNAi, RNA interference; siRNA, small interfering RNA.

scrambled negative control and GalNAc-T3 were 5′-TTCTC CGAACGTGTCACGT-3′ and 5′-GGTCTGATCACTGCTC GGT-3′, respectively. S2-013 cells were transfected with an empty Neo-pSUPERgfp, a scrambled oligo-pSUPERgfp negative control or a plasmid designed to express the siRNA to GalNAc-T3, using FuGENE6 (Roche, Penzberg, Germany). The cells were selected in medium containing 500 μg/ml geneticin to generate stable pSUPERgfp cell lines. Single clones were isolated and analyzed for protein levels by western blotting.

Mice and xenografts

Female athymic nude mice (NCr-nu/nu) at 7 weeks of age and specifically pathogen-free were purchased from the National Cancer Institute. The mice were treated in accordance with the Institutional Animal Care and Use Committee guidelines. A suspension containing 8×10^5 stable control cells (2 clones, total 10 mice) or the GalNAc-T3 RNAi (2 clones, total 10 mice) derivative from S2-013 cells in 50 μl of Hank's balanced Salt Solution was injected subcutaneously into the dorsa of mice at the proximal midline. The tumors were measured every 5–7 days in two diameters using a dial caliper. Volumes were determined using the formula $a^2 \times b \times 0.52$ (where *a* is the shortest and *b* is the longest diameter). All mice were killed at the completion of the experiment and tumors were fixed in 10% buffered formalin and embedded in paraffin.

Flow cytometric analysis of apoptosis

Stable control and GalNAc-T3 RNAi cells of S2-013 were analyzed for apoptotic cell population by flow cytometry as described previously (Joshi *et al*., 2001). Briefly, 1×10^6 cells were harvested by trypsinization and fixed in 70% ethanol. The cells were resuspended in 1 ml of Telford reagent containing EDTA (33.62 μg), RNase-A (2.5 U), propidium iodide (50 μg), Triton X-100 (1.0 μl) and phosphate-buffered saline (to a total volume of 1 ml). The cells were incubated at 4 °C for 24 h and analyzed with a BD FACSCalibur flow cytometer (Becton Dickinson, Franklin Lakes, NJ, USA) using the Cell Quest Acquisition Software (Becton Dickinson) for data acquisition. Following data collection, cell-cycle distribution and apoptosis were modeled using ModFit LT (Verity Software House, Topsham, ME, USA; Gray and Dean, 1980). The correlation between the flow cytometric data that measures the apoptotic peak and DNA laddering has been described previously (Telford *et al*., 1991).

In situ *TUNEL assay*

Manifestations of cell death were observed using fluorescent *in situ* TUNEL staining. Cells were fixed with 4% formaldehyde and the TUNEL reaction mixture was obtained by adding terminal deoxynucleotidyl transferase to a nucleotide mixture, as instructed by the manufacturer's manual (Roche). The cells were then incubated with 50 μl of the TUNEL reaction mixture at 37 °C in the dark for 60 min. After rinsing with phosphate-buffered saline, the nuclei of the specimens were counterstained with 4,6-diamidino-2-phenylindole (DAPI) and visualized with a Zeiss LSM510 META microscope (Carl Zeiss, Gottingen, Germany).

Cytosol and membrane fractionation

Cells were homogenized in hypotonic buffer (20 mM Tris–HCl (pH 8.0), 150 mM NaCl, 1 mM EDTA, 1 mM phenylmethylsulphonyl fluoride, 1 mM Na_3VO_4) using a Dounce homogenizer,

centrifuged at 700 *g* for 5 min and the post-nuclear supernatant was then centrifuged at 100 000 *g* for 1 h. The resulting supernatant was collected and used as the cytosolic fraction. The pellet was resuspended in hypotonic buffer containing 1% Triton X-100 and incubated on ice for 1 h. The supernatant component (particulate fraction) was centrifuged at 14 000 *g* for 20 min. Protein concentrations were determined by the Bio-Rad protein assay using bovine serum albumin as a standard.

MS analysis
The membrane fractions from the stable scrambled negative control and GalNAc-T3 RNAi S2-013 cells were separated by 4–20% gradient sodium dodecyl sulfate–PAGE and silver-stained. Bands that distinguished the proteins by knockdown of GalNAc-T3 from those in control cells were excised, digested in-gel with trypsin and analyzed using a Q-TOF Ultima tandem mass spectrometer (Waters, Milford, MA, USA) with electrospray ionization. Database searches of the acquired MS/MS spectra were performed using MASCOT v1.9.0 (Matrix Science, London, UK).

Enzyme treatment
Total cell lysates were treated with 0.2 U/ml of sialidase (Roche) for 4 h at 37 °C, 100 U of peptide *N*-glycosidase-F (New England Biolabs, Ipswich, MA, USA) for 1 h at 37 °C, or 120 μg/ml *O*-sialoglycoprotein endopeptidase (Cedarlane, Burlington, Ontario, Canada) for 4 h at 37 °C and then analyzed by western blotting using an anti-GNAT1 antibody.

Detection of sugar chains of GNAT1
S2-013 cells were lysed in lysis buffer (20 mM HEPES (pH 7.4), 100 mM KCl, 5 mM $MgCl_2$, 0.5% Triton X-100 and protease inhibitor cocktail tablets (Roche)) and incubated with 2 μg of anti-GNAT1 antibody and protein-G–Sepharose. Glycochains of GNAT1 were detected by using a commercially available kit, G.P. Sensor (Honen, Tokyo, Japan). After analysis of immunoprecipitated GNAT1 by western blotting, GNAT1 immobilized on a polyvinylidene difluoride membrane was subjected to periodate oxidation. The aldehyde group formed by the periodate oxidations was coupled with biotin hydrazide. Biotin hydrazide-sugar chains were then coupled with a streptavidin–horseradish peroxidase conjugate. The horseradish peroxidase-labeled glycochains of GNAT1 were detected by enhanced chemiluminescence.

siRNA treatment
RNAi targeting GNAT1 and scrambled negative control siRNA oligonucleotides were purchased from Santa Cruz Biotechnology (43783 and 37007; Santa Cruz, CA, USA). To examine the effect of the siRNAs on GNAT1 expression, S2-013 cells that expressed GNAT1 and PANC-1 cells that did not express GNAT1 were plated in six-well plates. After 20 h, the cells were transfected with 80 pmol of siRNA in an siRNA transfection reagent (Santa Cruz Biotechnology) following the manufacturer's instructions. After 72 h of incubation, the cells were used for western blot analysis and MTT assays.

Conflict of interest

The authors declare no conflict of interest.

Acknowledgements

We thank Michel Ouellette for providing the HPNE cells and Tamotsu Takeuchi for supporting pathological experiments and helpful discussion. We also thank Janice Taylor and James Talaska for excellent technical assistance. This work was funded by the NIH with grants to MAH (U01CA111294; R01CA057362).

References

Alenzi FQ. (2004). Links between apoptosis, proliferation and the cell cycle. *Br J Biomed Sci* **61**: 1–4.

Andersen MH, Becker JC, Straten P. (2005). Regulators of apoptosis: suitable targets for immune therapy of cancer. *Nat Rev Drug Discov* **4**: 399–409.

Bennett EP, Hassan H, Clausen H. (1996). cDNA cloning and expression of a novel human UDP-*N*-acetyl-alpha-D-galactosamine. Polypeptide *N*-acetylgalactosaminyltransferase, GalNAc-T3. *J Biol Chem* **271**: 17006–17012.

Braga VM, Pemberton LF, Duhig T, Gendler SJ. (1992). Spatial and temporal expression of an epithelial mucin, Muc-1, during mouse development. *Development* **115**: 427–437.

Brockhausen I. (1999). Pathways of *O*-glycan biosynthesis in cancer cells. *Biochim Biophys Acta* **1473**: 67–95.

Cattoretti G, Becker M H, Key G, Duchrow M, Schluter C, Galle J *et al.* (1992). Monoclonal antibodies against recombinant parts of the Ki-67 antigen (MIB1 and MIB3) detect proliferating cells in microwave-processed formalin-fixed paraffin sections. *J Pathol* **168**: 357–363.

Fuster MM, Esko JD. (2005). The sweet and sour of cancer: glycans as novel therapeutic targets. *Nat Rev Cancer* **5**: 526–542.

Gray JW, Dean PN. (1980). Display and analysis of flow cytometric data. *Annu Rev Biophys Bioeng* **9**: 509–539.

Hakomori S. (1989). Aberrant glycosylation in tumors and tumor-associated carbohydrate antigens. *Adv Cancer Res* **52**: 257–331.

Hollingsworth MA, Swanson BJ. (2004). Mucins in cancer: protection and control of the cell surface. *Nat Rev Cancer* **4**: 45–60.

Iwamura T, Katsuki T, Ide K. (1987). Establishment and characterization of a human pancreatic cancer cell line (SUIT-2) producing carcinoembryonic antigen and carbohydrate antigen 19-9. *Jpn J Cancer Res* **78**: 54–62.

Jemal A, Siegel R, Ward E, Hao Y, Xu J, Thun MJ. (2009). Cancer statistics, 2009. *CA Cancer J Clin* **59**: 225–249.

Jensen ON. (2006). Interpreting the protein language using proteomics. *Nat Rev Mol Cell Biol* **7**: 391–403.

Joshi SS, Kuszynski CA, Bagchi D. (2001). The cellular and molecular basis of health benefits of grape seed proanthocyanidin extract. *Curr Pharm Biotechnol* **2**: 187–200.

Kannagi R, Izawa M, Koike T, Miyazaki K, Kimura N. (2004). Carbohydrate-mediated cell adhesion in cancer metastasis and angiogenesis. *Cancer Sci* **95**: 377–384.

Kondo A, Li W, Nakagawa T, Nakano M, Koyama N, Wang X *et al.* (2006). From glycomics to functional glycomics of sugar chains: identification of target proteins with functional changes using gene targeting mice and knock down cells of FUT8 as examples. *Biochim Biophys Acta* **1764**: 1881–1889.

Lee KM, Yasuda H, Hollingsworth MA, Ouellette MM. (2005). Notch2-positive progenitors with the intrinsic ability to give rise to pancreatic ductal cells. *Lab Invest* **85**: 1003–1012.

Li M, Song L, Qin X. (2010). Glycan changes: cancer metastasis and anticancer vaccines. *J Biosci* **35**: 665–673.

Mayoral MA, Mayoral C, Meneses A, Villalvazo L, Guzman A, Espinosa B *et al.* (2008). Identification of galectin-3 and mucin-type

O-glycans in breast cancer and its metastasis to brain. *Cancer Invest* **26**: 615–623.

Mellors A, Lo RY. (1995). *O*-sialoglycoprotease from *Pasteurella haemolytica*. *Methods Enzymol* **248**: 728–740.

Merighi S, Benini A, Mirandola P, Gessi S, Varani K, Leung E *et al.* (2006). Modulation of the Akt/Ras/Raf/MEK/ERK pathway by A(3) adenosine receptor. *Purinergic Signal* **2**: 627–632.

Moniaux N, Andrianifahanana M, Brand RE, Batra SK. (2004). Multiple roles of mucins in pancreatic cancer, a lethal and challenging malignancy. *Br J Cancer* **91**: 1633–1638.

Nomoto M, Izumi H, Ise T, Kato K, Takano H, Nagatani G *et al.* (1999). Structural basis for the regulation of UDP-*N*-acetyl-alpha-D-galactosamine: polypeptide *N*-acetylgalactosaminyl transferase-3 gene expression in adenocarcinoma cells. *Cancer Res* **59**: 6214–6222.

Reis CA, David L, Correa P, Carneiro F, de Bolos C, Garcia E *et al.* (1999). Intestinal metaplasia of human stomach displays distinct patterns of mucin (MUC1, MUC2, MUC5AC, and MUC6) expression. *Cancer Res* **59**: 1003–1007.

Rosenzweig DH, Nair KS, Wei J, Wang Q, Garwin G, Saari JC *et al.* (2007). Subunit dissociation and diffusion determine the subcellular localization of rod and cone transducins. *J Neurosci* **27**: 5484–5494.

Ruiz-Avila L, McLaughlin SK, Wildman D, McKinnon PJ, Robichon A, Spickofsky N *et al.* (1995). Coupling of bitter receptor to phosphodiesterase through transducin in taste receptor cells. *Nature* **376**: 80–85.

Spiro RG. (2002). Protein glycosylation: nature, distribution, enzymatic formation, and disease implications of glycopeptides bonds. *Glycobiology* **12**: 43R–56R.

Sutherlin ME, Nishimori I, Caffrey T, Bennett EP, Hassan H, Mandel U *et al.* (1997). Expression of three UDP-*N*-acetyl-alpha-D-galactosamine:polypeptide GalNAc *N*-acetylgalactosaminyltransferases in adenocarcinoma cell lines. *Cancer Res* **57**: 4744–4748.

Takenaka Y, Fukumori T, Raz A. (2004). Galectin-3 and metastasis. *Glycoconj J* **19**: 543–549.

Telford WG, King LE, Fraker PJ. (1991). Evaluation of glucocorticoid-induced DNA fragmentation in mouse thymocytes by flow cytometry. *Cell Prolif* **24**: 447–459.

White T, Bennett EP, Takio K, Sorensen T, Bonding N, Clausen H. (1995). Purification and cDNA cloning of a human UDP-*N*-acetyl-alpha-D-galactosamine: polypeptide *N*-acetylgalactosaminyltransferase. *J Biol Chem* **270**: 24156–24165.

Wray CJ, Ahmad SA, Matthews JB, Lowy AM. (2005). Surgery for pancreatic cancer: recent controversies and current practice. *Gastroenterology* **128**: 1626–1641.

Supplementary Information accompanies the paper on the Oncogene website (http://www.nature.com/onc)

BART inhibits pancreatic cancer cell invasion by inhibiting ARL2-mediated RhoA inactivation

KEISUKE TANIUCHI, SHINJI IWASAKI and TOSHIJI SAIBARA

Department of Gastroenterology and Hepatology, Kochi University Medical School, Nankoku, Kochi 783-8505, Japan

Received May 2, 2011; Accepted June 10, 2011

DOI: 10.3892/ijo.2011.1156

Abstract. We report that BART plays a role in inhibiting cell invasion by regulating the activity of the Rho GTPase protein RhoA in pancreatic cancer cells. BART was originally identified as a binding partner of ARL2, a small G-protein implicated as a regulator of microtubule dynamics and folding. We show that BART interacts with GTP-bound ARL2 and is required for the binding of GTP-bound ARL2 with active forms of RhoA at leading edges in migrating cancer cells. GTP-bound ARL2 inactivates RhoA and BART prevents ARL2 from regulating RhoA activity. Thus, BART binds to and functions as an inhibitor of ARL2 at leading edges of migrating cells, thereby increasing the amount of active RhoA. Treatment with the Rho inhibitor C3 exoenzyme induces cell invasion by pancreatic cancer cells to the same level as that of cells in which BART is stably knocked down by RNA interference. GTP-bound ARL2 acts as a RhoA inhibitor by a mechanism that involves the induction of actin-cytoskeleton rearrangements. We show that BART decreases actin-cytoskeleton rearrangements by inhibiting ARL2 function and by increasing the amount of active RhoA in pancreatic cancer cells. Our results imply that BART increases active RhoA by inhibiting ARL2 function, which in turn inhibits invasiveness of cancer cells.

Introduction

Binder of Arl Two (BART) is a soluble 19-kDa protein that was originally purified from bovine brain and identified as a binding partner of small G-protein ADP-ribosylation factor-like 2 (ARL2) (1). ARL proteins lack the biochemical and genetic activities characteristic of the ADP-ribosylation factor (ARF) family, despite the 40-60% identity between ARF and ARL proteins (2). ARL2 has been implicated as a regulator of microtubule dynamics and folding (3), but its function remains largely unknown. Nuclear magnetic resonance analysis recently showed that BART forms a novel fold composed of six α-helices that form three interlocking L shapes (4). GTP-ARL2 assumes a typical small GTPase fold with a unique N-terminal α-helix conformation (5). The regions involved in the binding of ARL2 to its protein partners localize to these loop regions (4). The interactions between ARL2 and BART involve two interfaces: a conserved N-terminal LLXIL motif of ARL2 embedded in a hydrophobic cleft of BART, and the switch regions of ARL2 that interact with helix α3 of BART (5). This novel partner recognition and binding mode is different from that of other small GTPase-effector interactions and provides the molecular basis for the high specificity of ARL2-BART binding (5).

BART interaction with ARL2 affects the transcriptional activity and nuclear retention of signal transducer and activator of transcription 3 (STAT3), which is both a cytoplasmic signaling molecule and a nuclear transcription factor (6). Recent studies have linked STAT3 to the metastatic progression of several different cancer types. Studies using mouse embryo fibroblasts established STAT3 as a component of the Rho GTPase-signaling cascade (7,8). Rho GTPases are important regulators of both actin dynamics and cell-substratum adhesions in migratory cells, and are therefore critical in the process of tumor invasion and angiogenesis (9). Although the mechanisms that contribute to the constitutive activation of STAT3 in cancer invasion and metastasis are currently unclear, the binding of BART to ARL2 might contribute to the function of cell migration through the Rho GTPase-signaling cascade.

We previously reported that regulation of BART post-transcriptional modification via intracellular CD24 binding to G3BP in stress granules contributes to inhibition of invasion and metastasis of pancreatic ductal adenocarcinoma (PDAC) cells (10). In this study, we report the mechanism by which BART regulates RhoA activity through its binding to ARL2 in PDAC cells. GTP-bound ARL2 directly binds to active forms of RhoA and plays a role in inhibiting activation of RhoA. BART forms a complex with ARL2 and RhoA, resulting in the promotion of GTP-RhoA loading in PDAC cells. Consequently, BART prevents ARL2 from regulating RhoA activity and thereby inhibits cell invasion by restricting surface rearrangements of the actin cytoskeleton.

Correspondence to: Dr Keisuke Taniuchi, Department of Gastroenterology and Hepatology, Kochi University Medical School, Nankoku, Kochi 783-8505, Japan
E-mail: jm-ktaniuchi@kochi-u.ac.jp

Abbreviations: PDAC, pancreatic ductal adenocarcinoma; siRNA, small interfering RNA; RhoGAP, Rho GTPase-activating proteins

Key words: small G-protein, Rho GTPase, pancreatic cancer, cell invasion, actin-cytoskeleton

Materials and methods

Cell culture. The human PDAC cell line S2-013, a subline of SUIT-2, was obtained from Dr T. Iwamura (Miyazaki Medical College, Miyazaki, Japan) (11). The human PDAC cell line PANC-1 was obtained from the ATCC. Cells were grown in Dulbecco's modified Eagle's medium (DMEM; Gibco-BRL, Carlsbad, CA) supplemented with 10% heat-inactivated fetal calf serum (FCS) at 37˚C saturated with 5% CO_2 in a humid atmosphere.

Antibodies. Rabbit anti-BART antibody (MGC1121) was purchased from ProteinTech (Chicago, IL). Goat anti-ARL2 antibody (IMG-3515) was obtained from Imgenex (San Diego, CA). Monoclonal antibodies against RhoA (26C4), myc (9E10), and rabbit anti-myc antibody (A14) were purchased from Santa Cruz Biotechnology (Santa Cruz, CA). Monoclonal antibody against Rac1 (610650) was obtained from BD Transduction Laboratory (Palo Alto, CA).

In vivo binding of BART with ARL2. The entire cDNA coding sequence of wild-type ARL2 was amplified by RT-PCR and the product was inserted into pcDNA3.1(+)/myc-His A (Invitrogen, Carlsbad, CA). The myc-tagged ARL2 construct was transiently transfected into S2-013 cells using FuGENE6 (Roche, Penzberg, Germany), according to the manufacturer's instructions. At 48 h after transfection, the cells were lysed in lysis buffer [20 mM HEPES (pH 7.4), 100 mM KCl, 5 mM $MgCl_2$, 0.5% Triton X-100, protease inhibitor cocktail tablets (Roche)] and immunoprecipitated with 2 μg of anti-myc or anti-BART antibody. The interaction of myc-ARL2 with endogenous BART as an immune complex was analyzed by Western blotting with anti-myc and anti-BART antibodies.

Confocal immunofluorescence microscopy. Cells were fixed with 4% paraformaldehyde, permeabilized with 0.1% Triton X-100, covered with blocking solution (3% BSA/PBS), and then incubated with the primary antibody for 1 h. Alexa 488, Alexa 546, Alexa 594 and Alexa 633-conjugated secondary antibodies (Molecular Probes, Carlsbad, CA) were used with or without rhodamine phalloidin (Cytoskeleton, Denver, CO). Each specimen was visualized with a Zeiss LSM 510 META microscope (Carl Zeiss, Gottingen, Germany).

Affinity precipitation of BART and RhoA with GST-ARL2. The entire cDNA coding sequence of wild-type ARL2 was inserted into the pGEX-6P1 vector (GE Healthcare, Piscataway, NJ). The GST-ARL2 fusion protein was produced in *Escherichia coli*, purified with glutathione-Sepharose beads, and used for affinity precipitation in a GST-pull-down assay. S2-013 cells were lysed in lysis buffer and equal amounts of total lysate were incubated with 8 μg of the GST-ARL2 fusion protein at 4˚C for 1 h. GST was used as a control. Western blotting was performed to detect co-precipitated BART and RhoA using anti-BART and anti-RhoA antibodies, respectively.

Wound healing immunostaining assay. Cells were transfected with the indicated plasmids using FuGENE6. At 48 h after transfection, a wound in the form of a cross was made through the confluent cell monolayer with a plastic pipette tip and the cells were then allowed to polarize and migrate toward the wound. After 4 h, the cells were immunostained with the primary antibody and then incubated with fluorophore-conjugated secondary antibodies as described above. Each specimen was visualized with a Zeiss LSM 510 META microscope.

Affinity precipitation using a GST-bound RhoA interactive binding domain. The pGEX-6P1 plasmids encoding p21-activated kinase (PAK)-Cdc42/Rac interactive binding (CRIB) domain or Rhotekin were kindly provided by Dr K. Johnson (University of Nebraska Medical Center, Omaha, NE). These GST fusion proteins were purified with glutathione-Sepharose beads and used for affinity precipitation in GST-pull-down assays to estimate the activity of Rac1 and RhoA. Cells were transfected with the indicated plasmids using FuGENE6. At 48 h after transfection, equal amounts of protein from each cell lysate were incubated with 8 μg of GST-fusion protein, and the bound proteins were detected by Western blotting using anti-Rac1 or anti-RhoA antibodies.

Small interfering RNA-expressing constructs and the generation of stable cell lines. Small interfering RNA-methodologies were performed as previously reported (10).

Inhibition of endogenous RhoA by the Rho inhibitor C3 exoenzyme. The Rho inhibitor C3 exoenzyme from *Clostridium botulinum* (Calbiochem, San Diego, CA) was introduced into cells using FuGENE6. Briefly, 20 μg/ml C3 exoenzyme was mixed with FuGENE6 in medium lacking FCS and incubated with cells for 14 h at 37˚C before GST-Rhotekin pull-down and Matrigel invasion assays were performed, as described below.

Matrigel invasion assay. A two-chamber invasion assay was used to assess cell invasion (24-well plates, 8 μm pore size, membrane coated with a layer of Matrigel extracellular matrix proteins; Becton-Dickinson, San Jose, CA). First, $4.0x10^4$ cells were seeded in serum-free medium into the upper chamber and allowed to invade toward 5% FCS as a chemoattractant in the lower chamber. After 20 h of incubation, the number of invading cells at the bottom of the membrane was estimated by counting three independent visual fields under a microscope.

BART-rescue construct. The entire coding sequence of BART cDNA was amplified by RT-PCR. The product was subsequently inserted into the pCMV6 Entry vector (Origene, Rockville, MD) bearing a C-terminal myc-DDK-tag. This BART-rescue construct was transiently transfected into cells using FuGENE6 (Roche).

Immunoprecipitation. S2-013 cells were transfected with the indicated myc-tagged plasmids using FuGENE6. After 48 h, the cells were lysed in lysis buffer and equal amounts of cell lysate were incubated with 2 μg of the indicated antibody or control IgG monoclonal antibody (isotype control) and protein G Sepharose. Co-immunoprecipitated proteins were detected by Western blotting using the indicated antibodies.

GST-mutant ARL2 binding assay in vitro. The pET23b plasmids encoding ARL2-Q70L or ARL2-T30N, with the indicated ARL2 amino acid substitutions (numbers refer to the corre-

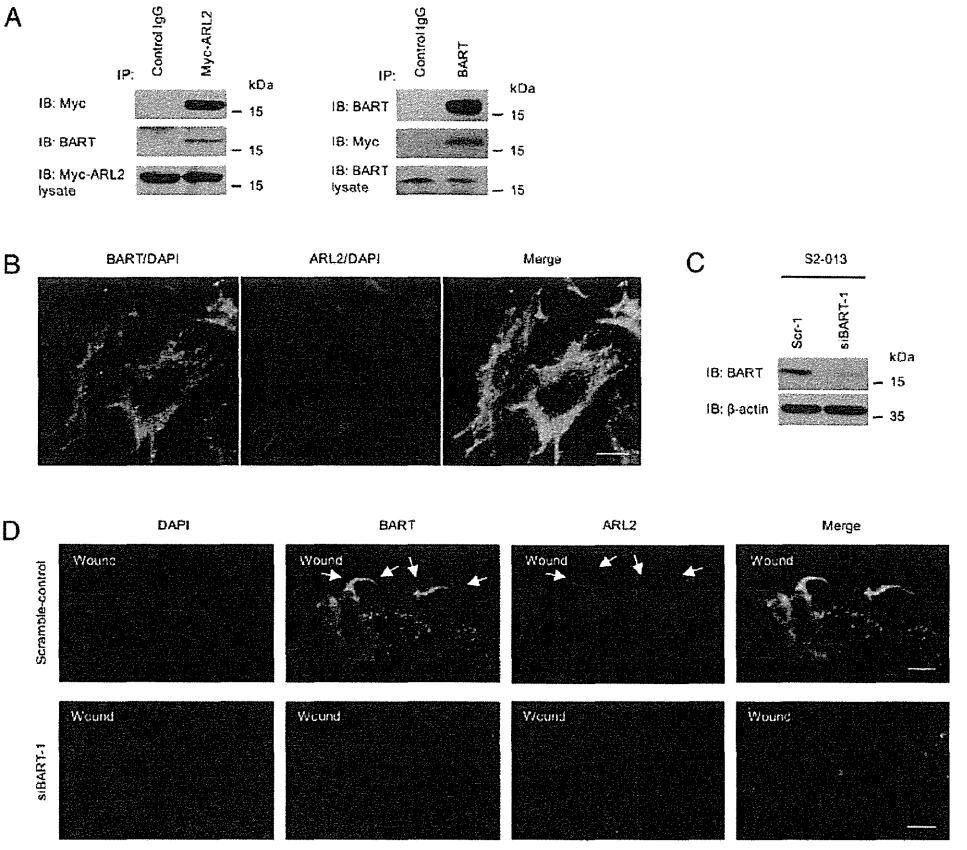

Figure 1. BART binds to ARL2 at the leading edges of migrating cells. (A) Immunoprecipitation of endogenous BART or exogenous ARL2 from S2-013 cells. A myc-tagged ARL2 construct was transiently transfected into S2-013 cells and immunoprecipitated with anti-myc or anti-BART antibodies. Immunoprecipitates were examined by Western blotting using anti-BART and anti-myc antibodies. Rabbit IgG was used as an isotype control. (B) Immunocytochemical staining of S2-013 cells using anti-BART (green) and anti-ARL2 (red) antibodies. Blue, DAPI staining. Bar, 10 μm. (C) Western blot analysis using the anti-BART antibody showing one representative clone of S2-013 cells transfected with siRNA for BART (siBART-1) as compared to a scrambled control clone (Scr-1). (D) Confluent scramble-control (upper panels) and BART RNAi S2-013 cells (lower panels) were wounded. After 4 h, the cells were immunostained with anti-BART (green) and anti-ARL2 (red) antibodies. Blue, DAPI staining. Arrows, colocalized BART and ARL2 at the leading edge. Bars, 10 μm.

sponding amino acids in ARL2), were kindly provided by Dr N. Cowan (New York University Medical Center, New York, NY) (12). GST-ARL2-Q70L and GST-ARL2-T30N were constructed by subcloning mutant ARL2 from the pET23b plasmids into pGEX-6P1 and subsequent confirmation of the DNA sequence. GST-ARL2-Q70L and T30N fusion proteins were produced in *E. coli* and purified as described above. Six micrograms of His-tagged wild-type RhoA protein (Cytoskeleton) was incubated with either GTPγS or with GDP at a final concentration of 1 mM in 20 μl of reaction buffer [50 mM HEPES (pH 7.4), 100 mM NaCl, 10 mM $MgCl_2$, 5 mM EDTA, 1 mM DTT] at 30°C for 15 min. The concentration of $MgCl_2$ was then increased to 50 mM $MgCl_2$, and 8 μg of GST-tagged Q70L or T30N was added and incubated at 4°C for 4 h. GST was used as a control. After the beads were extensively washed with lysis buffer, bound RhoA was detected by Western blotting using an anti-RhoA antibody.

In vitro Rho-GAP assay. Wild-type ARL2 that was fused to GST as described above, was released by cleavage with factor Xa as previously reported (13). *In vitro* GAP assays were performed in triplicate using the RhoGAP Assay Biochem Kit (Cytoskeleton). His-tagged RhoA (5 μg) was incubated with wild-type ARL2 protein (8 μg) and 200 μM GTP with or without p50 RhoGAP protein (8 μg) at 37°C for 20 min in a reaction mixture (20 μl) containing 25 mM HEPES (pH 7.4), 100 mM NaCl, 2 mM $MgCl_2$ and 1 mM DTT. Phosphate generated by hydrolysis of GTP was measured by adding CytoPhos reagent (Cytoskeleton) and the absorbance was read at 650 nm.

Statistical analysis. The significance of differences between groups was determined using Student's t-test, the Mann-Whitney U test or Fisher's exact test, as appropriate. $P<0.05$ was considered statistically significant.

Results

Colocalization of BART and ARL2 in PDAC cells. To confirm the interaction of BART and ARL2 in PDAC cells, we performed co-immunoprecipitation experiments. The myc-tagged ARL2 construct was transfected into human PDAC S2-013 cells, and exogenous ARL2 and endogenous BART were immunoprecipitated using anti-myc and anti-BART antibodies, respectively. Immunoblotting of the precipitates revealed that myc-ARL2 co-immunoprecipitated with endogenous BART (Fig. 1A). We next examined the subcellular

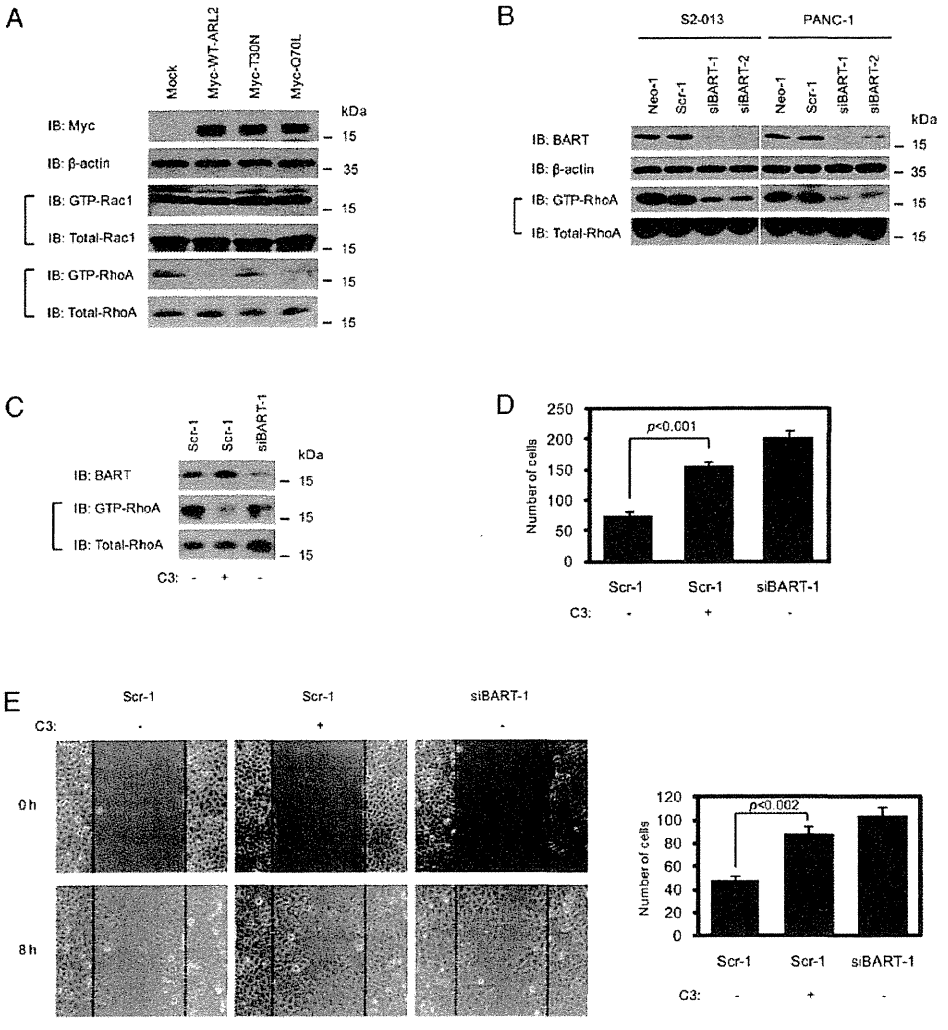

Figure 2. BART and GTP-ARL2 modulates RhoA activity, and RhoA is associated with cell invasion. (A) Myc-tagged wild-type ARL2 or its point mutants Q70L and T30N were transiently transfected into S2-013 cells and the amount of active, GTP-loaded Rac1 and RhoA were determined by GST-pull-down assays using GST-PAK-CRIB and GST-Rhotekin, respectively. Precipitates were examined by Western blotting using anti-Rac1 and anti-RhoA antibodies. (B) Western blotting with the anti-BART antibody showing each two representative clones (siBART-1 and 2) of S2-013 and PANC-1 cells transfected with BART siRNA as compared to mock (Neo-1) and scrambled (Scr-1) control clones. The amount of active, GTP-loaded RhoA in the control and BART RNAi cells was determined using GST-pull-down assays with GST-Rhotekin. Precipitants were examined by Western blotting using anti-RhoA antibody. (C) Scramble-control cells of S2-013 were preloaded with or without C3 exoenzyme, and active RhoA was assessed by GST-pull-down assays using GST-Rhotekin, followed by Western blotting. (D) Scramble-control S2-013 cells pretreated with or without C3 exoenzyme and non-treated silenced BART S2-013 cells were plated on Matrigel invasion chambers. Invaded cells in four fields per group were counted. Data are representative of three independent experiments. Columns, mean; bars, SD. P-value as compared to non-treated scramble-control cells. (E) Confluent control and BART RNAi S2-013 cells were preloaded with or without C3 exoenzyme and wounded. The dashed lines indicate the border of the scratch (time 0), made using a plastic pipette tip. The number of cells which migrated into the initially cell-free scratch was counted. Cells in four defined areas per group were quantified for each experiment. Data are representative of three independent experiments. Columns, mean; bars, SD. P-value as compared to non-treated scramble-control cells.

localization of endogenous BART and ARL2 in S2-013 cells by immunofluorescence (Fig. 1B). Staining of BART and ARL2 colocalized in the cytoplasm.

To determine the effect of BART depletion on the localization of ARL2, plasmids expressing small interfering RNAs (siRNAs) specific for BART were stably expressed in S2-013 cells (Fig. 1C). A wound-healing assay was used to observe the localization of BART and ARL2 in polarized migrating cells (Fig. 1D). We confirmed that knockdown of BART in S2-013 and PANC-1 enhanced cell motility into a wounded area of confluent cultures compared to control cells (10). BART and ARL2 were both recruited to the leading edges during wound healing of control S2-013 cells (upper panels in Fig. 1D). However, depletion of BART inhibited the accumulation of ARL2 at the leading edges (lower panels in Fig. 1D). These results indicate that BART and ARL2 are associated with cell migration and that ARL2 localizes at the leading edges in a BART-dependent manner in migrating PDAC cells.

ARL2 decreases the level of active RhoA. We examined the effects of ARL2 on the activity of small G-protein members of the Rho family Rac1 and RhoA, which are important regulators of both actin dynamics and cell-substratum adhesions in migratory cells. Rho family small GTPases are central regulators of actin-based cell motility (13). The myc-tagged wild-type ARL2 and its point mutated forms, Q70L and T30N, were transiently

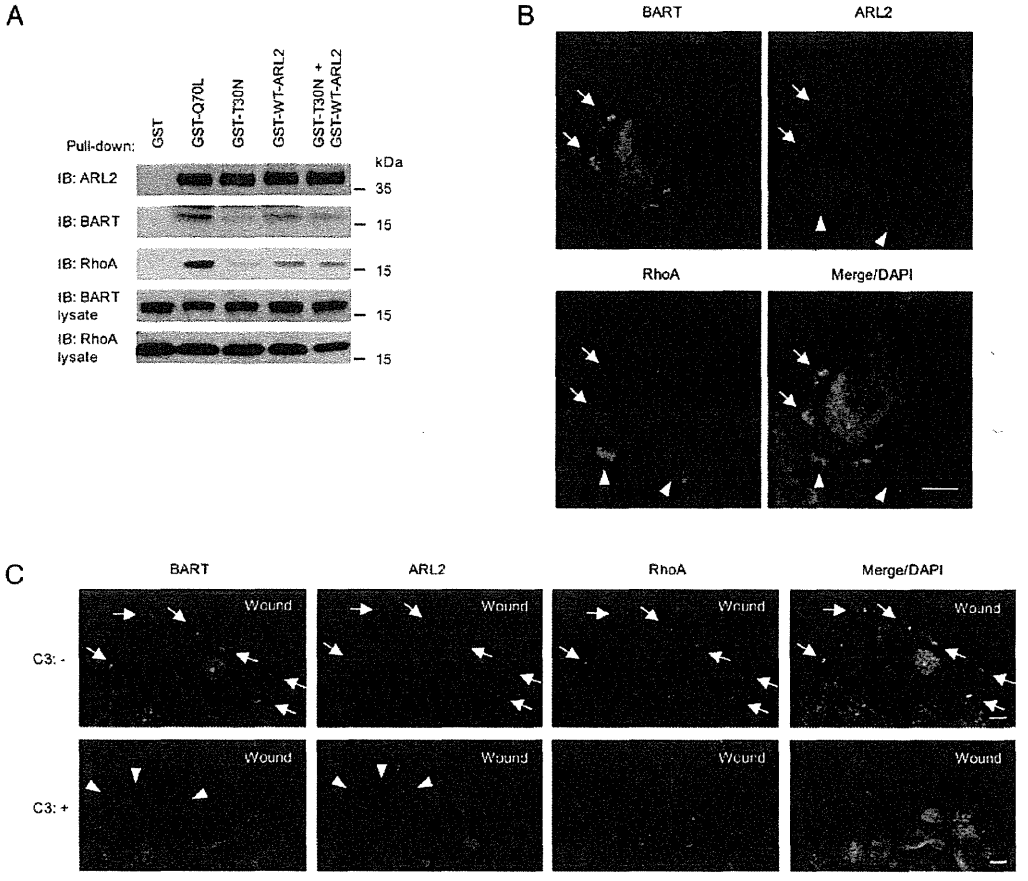

Figure 3. GTP-ARL2 binds to BART and active RhoA at cell protrusions in PDAC cells. (A) GST-bound wild-type and mutant ARL2 proteins were used for affinity precipitation in GST-pull-down assays. Equal amounts of S2-013 cell lysates were incubated with 8 μg of the GST-fusion protein, and the precipitated BART and RhoA were detected by Western blotting. (B) Immunocytochemical staining of S2-013 cells, using anti-BART (green), anti-ARL2 (red) and anti-RhoA (violet) antibodies. Blue, DAPI staining. Arrowheads, colocalized ARL2 and RhoA; arrows, colocalized BART, ARL2 and RhoA in lamellipodial-like protrusions. Bar, 10 μm. (C) S2-013 cells were preloaded with or without C3 exoenzyme, and immunocytochemical staining was performed, using anti-BART (green), anti-ARL2 (red) and anti-RhoA (violet) antibodies. Blue, DAPI staining. Arrows, colocalized BART, ARL2 and RhoA at the leading edge; arrowheads, colocalized BART and ARL2 at the leading edge. Bars, 10 μm.

transfected into S2-013 cells, followed by a GST-pull-down assay using GST-PAK-CRIB or GST-Rhotekin to estimate the level of active Rac1 and RhoA, respectively (Fig. 2A). The ARL2-Q70L mutant is GTPase defective (GTP-bound type), and the ARL2-T30N mutant is defective in GTP binding (GDP-bound type) (11). We found that, like wild-type ARL2, the GTP-bound form of ARL2-Q70L, decreased the amount of active RhoA, but it did not alter the amount of active Rac1. We infer from this result that, to prevent RhoA activation, ARL2 must be in the GTP-bound form. On the other hand, silencing of BART by siRNA in human PDAC S2-013 and PANC-1 cells caused a decrease in the level of active RhoA (Fig. 2B), suggesting that endogenous BART is associated with an increase in the level of active RhoA. These results suggest the possibility that the inactivation of RhoA by ARL2 might be inhibited by binding of BART to ARL2.

RhoA has been implicated in the regulation of directed cell migration (14). We next questioned whether RhoA influences PDAC cell migration and the potential role of BART in RhoA-mediated migration, by analyzing cell invasion of control and BART RNAi S2-013 cells after cell loading with the Rho inhibitor C3 exoenzyme. We first confirmed that loading of control S2-013 cells with the C3 exoenzyme decreased the level of GTP-RhoA (Fig. 2C). We previously reported that suppression of BART enhanced cell invasiveness in Matrigel invasion assays (10). Pretreatment of control S2-013 cells with C3 induced the same level of invasive activity in the Matrigel assay as that induced by knocking down BART (Fig. 2D). We also confirmed that C3 treatment of S2-013 cells enhanced cell motility into a wounded area of confluent cultures to the same level as that resulting from BART knockdown (Fig. 2E). Based on these results, we hypothesized that BART-dependent inhibition of PDAC cell invasion is likely to be associated with active RhoA via inhibition of GTP-ARL2 function.

BART is required for the binding of ARL2 to RhoA. Pull-down techniques were used to confirm the interaction between GST-tagged ARL2 (wild-type and its mutated forms, Q70L and T30N) and endogenous BART and RhoA in S2-013 cells (Fig. 3A). The binding of GST-ARL2-Q70L to BART and RhoA was enhanced compared to that of GST-wild-type ARL2, whereas the binding of GST-ARL2-T30N to BART and RhoA was significantly decreased. It is noteworthy that GST-pull-down using both GST-wild-type ARL2 and GST-ARL2-T30N

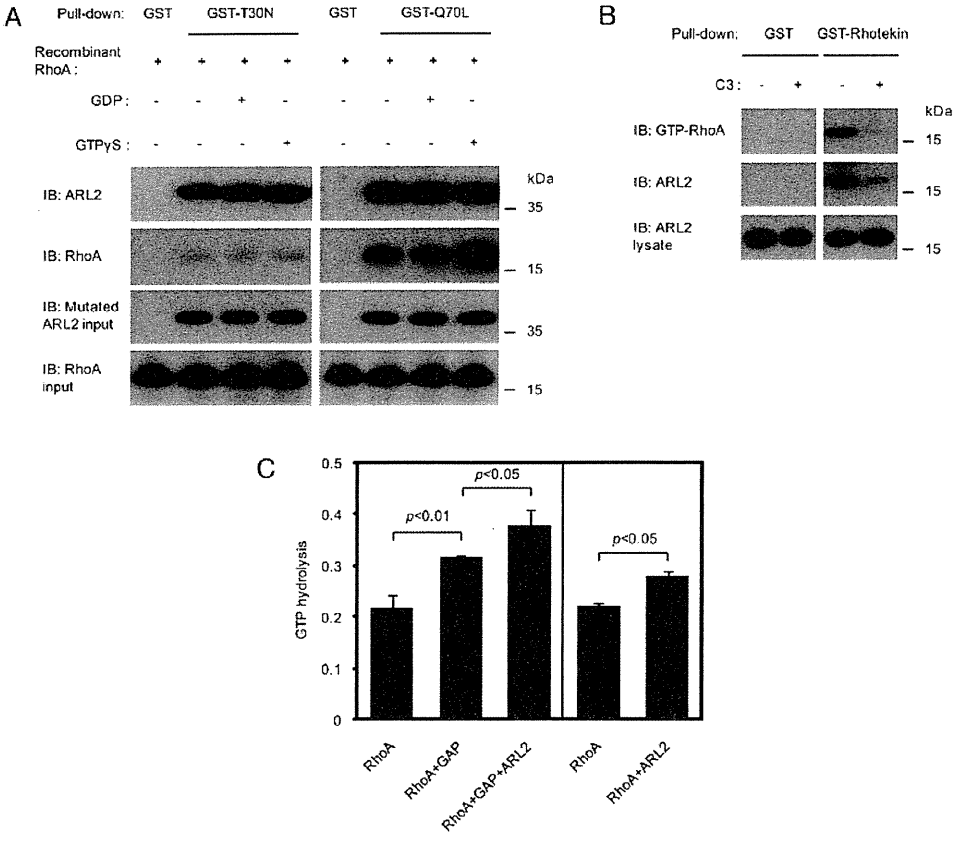

Figure 5. GTP-ARL2 interacts with GTP-RhoA and inactivates RhoA. (A) Incubation of recombinant RhoA with GDP or GTPγS was followed by pull-down experiments using GST-ARL2-Q70L or GST-ARL2-T30N. Precipitates were examined by Western blotting using anti-RhoA antibody. Data are representative of three independent experiments. (B) S2-013 cells were preloaded with or without C3 exoenzyme, and equal amounts of cell lysates were precipitated with GST-Rhotekin, followed by Western blotting with anti-ARL2 and anti-RhoA antibodies. Data are representative of three independent experiments. (C) To determine if wild-type ARL2 has a GAP function for RhoA GTPase, we carried out *in vitro* GAP assays using recombinant ARL2 protein produced in *Escherichia coli*. Data are representative of three independent experiments and are shown as means ± SEM.

ARL2 and RhoA was confirmed by immunoprecipitation with an anti-myc antibody (Fig. 4C). These results suggest that BART is necessary for the interaction and localization of active forms of ARL2 and RhoA at the front of the migrating cancer cells.

The active form of ARL2 binds to GTP-bound RhoA and inactivates RhoA. We used a second method to detect specific interaction between GTP-bound RhoA and the active form of ARL2. Recombinant RhoA that was incubated with GDP or GTPγS was used in pull-down experiments with GST-tagged ARL2-Q70L or ARL2-T30N (Fig. 5A). The amount of GTP-RhoA that bound to GST-ARL2-Q70L was significantly higher than that bound to GST-ARL2-T30N, which only weakly interacted with GTP-RhoA. Furthermore, pull-down assays of S2-013 cells using GST-Rhotekin, which binds to GTP-RhoA, pulled down both ARL2 and active RhoA. However, the level of ARL2 in the pull-downs decreased when C3 exoenzyme loaded cells were used, indicating that endogenous ARL2 interacts with active RhoA (Fig. 5B). These results confirmed that GTP-bound RhoA preferentially interacts with the active form of ARL2 in PDAC cells.

We hypothesized that RhoA might be a direct substrate of ARL2. Rho GTPase-activating proteins (RhoGAPs) stimulate the low intrinsic GTPase activity of Rho GTPase proteins, leading to conversion of GTP-bound active forms of Rho GTPases to GDP-bound inactive forms. In order to determine if wild-type ARL2 has GAP function, we performed *in vitro* GAP assays using recombinant wild-type ARL2 protein (Fig. 5C). We incubated recombinant ARL2 and human RhoA GTPase with or without the human p50 RhoGAP protein. The GAP domain from p50 RhoGAP stimulates GTPase activities of RhoA *in vitro*. In these studies, ARL2 also markedly increased the GTPase activity of RhoA (Fig. 5C). In addition, it is likely that ARL2 increased the GTPase activity of p50 RhoGAP towards RhoA (Fig. 5C). These results suggest that RhoA is the preferred substrate of ARL2 GAP activity.

BART inhibits the function of ARL2 in actin-cytoskeletal rearrangements. The Rho family constituting Rac1, Cdc42 and RhoA are important regulators of actin dynamics and cell-substratum adhesions in migratory cells, and thus are critically involved in cell motility and invasion (16-18). Moreover, active RhoA has been shown to be required for cadherin clustering in fibroblasts, suggesting that RhoA regulates cadherin-dependent cell adhesion (17). Phalloidin staining of F-actin showed that S2-013 cells transfected with myc-ARL2-Q70L extended many peripheral actin-rich structures in membrane

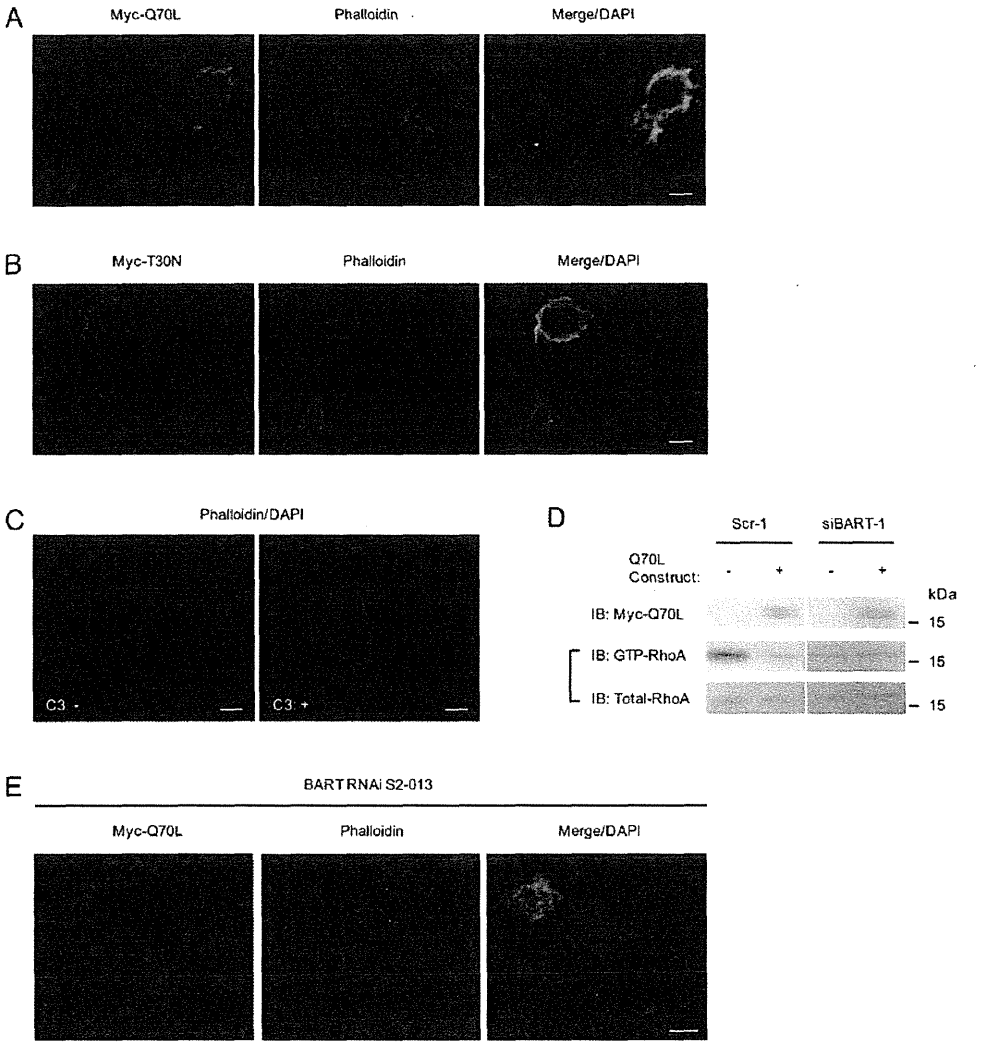

Figure 6. GTP-ARL2 induces actin-cytoskeleton rearrangements and BART inhibits the formation of an actin meshwork at protrusions through inhibition of ARL2 activity. (A) Immunocytochemical staining was performed 48 h after transfection of myc-tagged ARL2-Q70L into S2-013 cells using anti-myc antibody (green). The actin cytoskeleton (red) was stained with phalloidin. Blue, DAPI staining. Bar, 10 μm. (B) Immunocytochemical staining was performed 48 h after transfection of myc-tagged ARL2-T30N into S2-013 cells, using anti-myc antibody (green). Actin (red) was stained with phalloidin. Blue, DAPI staining. Bar, 10 μm. (C) S2-013 cells were preloaded with or without C3 exoenzyme and phalloidin staining was performed (red). Blue, DAPI staining. Bars, 10 μm. (D) The amount of active GTP-loaded RhoA was determined 48 h after transfection of myc-tagged ARL2-Q70L into control (Scr-1) and BART RNAi (siBART-1) cells, by GST-pull-down assays using GST-Rhotekin. GTP-RhoA was detected by Western blotting. (E) Immunocytochemical staining was performed 48 h after transfection of myc-tagged ARL2-Q70L into BART RNAi S2-013 cells (siBART-1) using anti-myc antibody (green). Actin was stained with phalloidin. Blue, DAPI staining. Bar, 10 μm.

ruffles at the edge of cell protrusions (Fig. 6A). Phalloidin staining of S2-013 cells transfected with myc-ARL2-T30N was similar to that of untransfected S2-013 cells (Fig. 6B). The myc-ARL2-T30N-expressing cells did not induce peripheral actin-cytoskeletal rearrangements. We confirmed that the C3 exoenzyme induced peripheral actin bundling in S2-013 cells (Fig. 6C). As seen in Fig. 2D and E, C3 loading induces invasive activity of PDAC cells. Thus, it is possible that RhoA inhibits cell invasion through the inhibition of peripheral actin-cytoskeletal rearrangements and that ARL2 plays an important role in regulating cell invasion. ARL2-Q70L is presumably primarily GTP-bound and inhibits activation of RhoA. Therefore, in order to induce peripheral actin-cytoskeletal rearrangements, ARL2 must be GTP-bound.

The overexpression of exogenous myc-tagged ARL2-Q70L in BART RNAi S2-013 cells did not induce any significant change in RhoA activity (Fig. 6D). This result indicates that BART modulates the function of GTP-bound ARL2 in RhoA inactivation. To investigate the role of BART and GTP-bound ARL2 in peripheral actin-cytoskeletal rearrangements, myc-tagged ARL2-Q70L was transfected into BART RNAi S2-013 cells (Fig. 6E). Overexpression of the exogenous myc-ARL2-Q70L mutant in BART RNAi cells had no obvious effect on the rearrangement of the actin-cytoskeleton. Thus, BART plays a role in preventing peripheral actin-cytoskeletal rearrangements caused by the expression of myc-ARL2-Q70L. These data reinforce our conclusion that BART increases the level of active RhoA, inhibits subsequent actin-cytoskeletal rearrangements by

inhibiting the function of GTP-bound ARL2 and thereby plays a role in inhibiting cell invasion.

Discussion

PDAC is among the most fatal of cancers due to its ability to extensively invade surrounding tissues and metastasize at an early stage (19). Extensive local infiltration and metastasis are the main causes of death in PDAC (20). Here, we examined the functional roles of BART and ARL2 in regulating cell migration in PDAC.

BART is a protein that binds ARL2, which belongs to the ARL family of proteins (1). In this study, we show that BART and ARL2 colocalize in the cytoplasm and accumulate at leading edges of PDAC cells. We found that depletion of BART diminished the accumulation of ARL2 at leading edges (Fig. 1D), indicating that BART is required for the recruitment of ARL2 to leading edges and that both BART and ARL2 are necessary for regulating the migration of PDAC cells.

To investigate the roles of ARL2 in modulation of the activity of Rho proteins, which are important regulators of both actin dynamics and cell-substratum adhesions in migratory cells, we performed GST pull-down assays using Rac1- and RhoA-binding domains. Experiments using GTPase-defective and GTP-binding-defective mutants of ARL2 revealed that GTP-ARL2 binds with active RhoA (Figs. 3A, 5A and B) and that it is the GTP-bound form of ARL2 that preferentially inhibits activation of RhoA (Fig. 2A). In contrast, when BART expression was suppressed, we found that the level of active RhoA was decreased (Fig. 2B), thus indicating that endogenous BART functions to positively regulate RhoA activity. The result that GTP-bound ARL2 is sufficient for decreasing the level of active RhoA in this system suggests that BART is likely to inhibit the function of GTP-ARL2 by directly binding to ARL2.

BART colocalizes with active forms of ARL2 and RhoA at leading edges of migrating PDAC cells (Fig. 3A and C). Knocking down of Smurf1, a HECT domain E3 ubiquitin ligase, induces colocalization of RhoA and F-actin in membrane protrusions and suppresses the tumorigenic morphology and motility of HEK293T cells (21). This result suggests that RhoA signaling is associated with dynamic membrane movement and inhibits cell motility. Depletion of BART diminished the accumulation of ARL2 and RhoA at leading edges (Fig. 4A), and their accumulation at leading edges was restored by the expression of myc-tagged BART (Fig. 4B). Preloading of control cells with the Rho inhibitor C3 exoenzyme induces invasive activity in Matrigel and wound-healing assays as efficiently as BART RNAi (Fig. 2D and E). Thus, decreased activity of RhoA induces cell invasion, and active RhoA is required for the anti-invasive activity of BART. On the basis of these results, it is most likely that BART is required for the binding of GTP-ARL2 to active RhoA at leading edges and that BART prevents GTP-ARL2 inhibition of RhoA and thereby inhibits cell invasion of PDAC cells. Further studies are needed to demonstrate the mechanism by which the trimeric BART/ARL2/RhoA complex is formed at the leading edge and by which direct binding of BART to ARL2 inhibits ARL2 activity.

The migratory competence of tumor cells requires activation of the motile cycle, the first step of which is actin remodeling, which drives the formation of cell protrusions, defines the direction of migration and initiates the growth of the lamellipodium (22). Dynamic actin remodeling processes at the leading edge of migrating cells are complex and involve increased actin filament severing, capping and dendritic branching (23). The concerted regulation of these events is mediated by a complex temporal and spatial interplay of Rho GTPases, kinases and phosphatases (22). Rho GTPases and their effectors are key intracellular signaling molecules that coordinate the cytoskeletal remodeling that is required for cell spreading, motility and cell-shape changes (24). The results of our immunofluorescence studies show that myc-ARL2-Q70L overexpression induces surface rearrangements of the actin cytoskeleton (Fig. 6A). Dynamic, actin-based plasma membrane protrusions that control growth cone path finding include lamellipodia, in which the actin cytoskeleton assumes a crosslinked and branched meshwork, and filopodia, which consist of parallel bundles of actin filaments protruding from the growth cone or lamellipodial margin (25). This result indicates that GTP-bound ARL2 is a physiological trigger that elicits redistribution of actin leading to peripheral actin-rearrangements. Interestingly, myc-ARL2-Q70L did not change the level of active RhoA in BART RNAi S2-013 cells (Fig. 6D). Additionally, peripheral actin-rearrangements were not induced when myc-ARL2-Q70L was overexpressed in BART RNAi S2-013 cells (Fig. 6E). Membrane ruffles and protrusions are characteristically present at the leading edge of motile cells, whereas stress fibers that promote adhesion to the substratum correlate negatively with cell locomotion (26). Inactivation of Rho kinase, by the Rho kinase inhibitor Y-27632 (27), leads to the dissolution of stress fibers and enhances cell movement during wound healing (15). Given the effect of the BART and ARL2 complex on peripheral actin-rearrangements, this complex must be associated with the regulation of membrane ruffles but not stress fibers, thereby allowing BART to inhibit cell invasion of PDAC cells through ARL2.

The findings presented in this study are supportive of the pivotal roles of BART and ARL2 in the coordinated regulation of cortical actin changes via the regulation of RhoA activity. We have established the functional significance of the interaction of BART with ARL2 in inhibition of the invasiveness of PDAC cells.

Acknowledgements

We thank Michael Hollingsworth for many helpful experimental suggestions. We also thank Keith Johnson for kindly providing us with the pGEX-Rhotekin and -PAK-CRIB plasmids, Nicholas Cowan for providing the pET23b-ARL2-Q70L and ARL2-T30N plasmids and Aki Tanouchi for her excellent technical assistance. This study was supported by a Grant-in-Aid from the Ministry of Health, Labour and Welfare of Japan (to T.S.).

References

1. Sharer JD and Kahn RA: The ARF-like 2 (ARL2)-binding protein, BART. Purification, cloning, and initial characterization. J Biol Chem 274: 27553-27561, 1999.
2. Clark J, Moore L, Krasinskas A, Way J, Battey J, Tamkun J and Kahn RA: Selective amplification of additional members of the ADP-ribosylation factor (ARF) family: cloning of additional human and Drosophila ARF-like genes. Proc Natl Acad Sci USA 90: 8952-8956, 1993.

3. Zhou C, Cunningham L, Marcus AI, Li Y and Kahn RA: Arl2 and Arl3 regulate different microtubule-dependent processes. Mol Biol Cell 17: 2476-2487, 2006.
4. Bailey LK, Campbell LJ, Evetts KA, Littlefield K, Rajendra E, Nietlispach D, Owen D and Mott HR: The structure of binder of Arl2 (BART) reveals a novel G protein binding domain: implications for function. J Biol Chem 284: 992-999, 2008.
5. Zhang T, Li S, Zhang Y, Zhong C, Lai Z and Ding J: Crystal structure of the ARL2-GTP-BART complex reveals a novel recognition and binding mode of small GTPase with effector. Structure 17: 602-610, 2009.
6. Muromoto R, Sekine Y, Imoto S, Ikeda O, Okayama T, Sato N and Matsuda T: BART is essential for nuclear retention of STAT3. Int Immunol 20: 395-403, 2008.
7. Aznar S, Valerón PF, Del Rincon SV, Pérez LF, Perona R and Lacal JC: Simultaneous tyrosine and serine phosphorylation of STAT3 transcription factor is involved in Rho A GTPase oncogenic transformation. Mol Biol Cell 12: 3282-3294, 2001.
8. Debidda M, Wang L, Zang H, Poli V and Zheng Y: A role of STAT3 in Rho GTPase-regulated cell migration and proliferation. J Biol Chem 280: 17275-17285, 2005.
9. Schmitz AA, Govek EE, Böttner B and van Aelst L: Rho GTPases: signaling, migration, and invasion. Exp Cell Res 261: 1-12, 2000.
10. Taniuchi K, Nishimori I and Hollingsworth MA: Intracellular CD24 inhibits cell invasion by post-transcriptional regulation of BART through interaction with G3BP. Cancer Res 71: 895-905, 2011.
11. Bhamidipati A, Lewis SA and Cowan NJ: ADP ribosylation factor-like protein 2 (Arl2) regulates the interaction of tubulin-folding cofactor D with native tubulin. J Cell Biol 149: 1087-1096, 2000.
12. Colinet D, Schmitz A, Depoix D, Crochard D and Poirié M: Convergent use of RhoGAP toxins by eukaryotic parasites and bacterial pathogens. PLoS Pathog 3: e203, 2007.
13. Hall A: Rho GTPases and the actin cytoskeleton. Science 279: 509-514, 1998.
14. Maekawa M, Ishizaki T, Boku S, Watanabe N, Fujita A, Iwamatsu A, Obinata T, Ohashi K, Mizuno K and Narumiya S: Signaling from Rho to the actin cytoskeleton through protein kinases ROCK and LIM-kinase. Science 285: 895-898, 1999.
15. Nobes CD and Hall A: Rho GTPases control polarity, protrusion, and adhesion during cell movement. J Cell Biol 144: 1235-1244, 1999.
16. Nobes CD and Hall A: Rho, Rac, and Cdc42 GTPases regulate the assembly of multimolecular focal complexes associated with actin stress fibers, lamellipodia, and filopodia. Cell 81: 53-62, 1995.
17. Takaishi K, Sasaki T, Kotani H, Nishioka H and Takai Y: Regulation of cell-cell adhesion by rac and rho small G proteins in MDCK cells. J Cell Biol 139: 1047-1059, 1997.
18. Etienne-Manneville S and Hall A: Rho GTPases in cell biology. Nature 420: 629-635, 2002.
19. Baumgart M, Heinmöller E, Horstmann O, Becker H and Ghadimi BM: The genetic basis of sporadic pancreatic cancer. Cell Oncol 27: 3-13, 2005.
20. Ahrendt SA and Pitt HA: Surgical management of pancreatic cancer. Oncology 16: 725-734, 2002.
21. Wang HR, Zhang Y, Ozdamar B, Ogunjimi AA, Alexandrova E, Thomsen GH and Wrana JL: Regulation of cell polarity and protrusion formation by targeting RhoA for degradation. Science 302: 1775-1779, 2003.
22. Eiseler T, Döppler H, Yan IK, Kitatani K, Mizuno K and Storz P: Protein kinase D1 regulates cofilin-mediated F-actin reorganization and cell motility through slingshot. Nat Cell Biol 11: 545-556, 2009.
23. Bamburg JR, McGough A and Ono S: Putting a new twist on actin: ADF/cofilins modulate actin dynamics. Trends Cell Biol 9: 364-370, 1999.
24. Ridley AJ: Rho GTPases and cell migration. J Cell Sci 114: 2713-2722, 2001.
25. Gallo G and Letourneau PC: Regulation of growth cone actin filaments by guidance cues. J Neurobiol 58: 92-102, 2004.
26. Boshans RL, Szanto S, van Aelst L and D'Souza-Schorey C: ADP-ribosylation factor 6 regulates actin cytoskeleton remodeling in coordination with Rac1 and RhoA. Mol Cell Biol 20: 3685-3694, 2000.
27. Uehata M, Ishizaki T, Satoh H, Ono T, Kawahara T, Morishita T, Tamakawa H, Yamagami K, Inui J, Maekawa M and Narumiya S: Calcium sensitization of smooth muscle mediated by a Rho associated protein kinase in hypertension. Nature 389: 990-994, 1997.

INTERNAL MEDICINE

□ ORIGINAL ARTICLE □

Serum Dehydroepiandrosterone Sulphate Levels in Patients with Non-Alcoholic Fatty Liver Disease

Masafumi Koga[1], Hiroshi Saito[1], Mikio Mukai[1], Toshiji Saibara[2] and Soji Kasayama[3]

Abstract

Backgound Dehydroepiandrosterone (DHEA) is an adrenal hormone reported to prevent body weight gain, diabetes mellitus and atherosclerosis. We hypothesized that DHEA is involved in the pathophysiology of non-alcoholic fatty liver disease (NAFLD) often associated with obesity and insulin resistance. In this study, we aimed to examine the clinical significance of serum DHEA sulfate (DHEAS) in patients with NAFLD.

Methods We determined serum DHEAS, serum alanine aminotransferase (ALT), serum lipids, plasma fasting glucose and insulin levels in 158 Japanese men who had neither viral hepatic diseases nor alcohol intake exceeding 20 g/day. NAFLD was diagnosed by the presence of fatty change of the liver by echotomographic examination.

Results Among the study subjects, 69 were diagnosed as having NAFLD. Their serum DHEAS levels were significantly higher than in 89 subjects without NAFLD. Serum DHEAS levels in 19 NAFLD patients with elevated ALT levels (>40 U/L) were significantly higher than in the other 50 NAFLD patients with normal ALT levels (≤40 U/L). Multivariate regression analysis demonstrated that serum ALT was positively correlated with serum DHEAS, serum triglyceride and body mass index.

Conclusion Serum DHEAS levels are increased in patients with NAFLD with elevated ALT levels. Increased serum DHEAS may be a component of the pathophysiology of NAFLD.

Key words: dehydroepiandrosterone, non-alcoholic fatty liver disease, fatty liver, alanine aminotransferase, non-alcoholic steatohepatitis

(Intern Med 50: 1657-1661, 2011)
(DOI: 10.2169/internalmedicine.50.4682)

Introduction

Non-alcoholic fatty liver disease (NAFLD) is the most common liver disease in affluent countries (1). Sometimes NAFLD progresses to non-alcoholic steatohepatitis (NASH) and liver cirrhosis (2-4). Some inflammatory cytokines and adipose tissue-derived cytokines are suggested to be involved in this progression (5-7) since the association of NAFLD with obesity and/or the metabolic syndrome has been indicated (8). This is also the case in subjects with hepatic steatosis. Although obesity and insulin resistance have been shown to play important roles in the development of NAFLD (9), the precise mechanisms for the progression from simple steatosis without elevated serum alanine aminotransferase (ALT) to that with elevated ALT remain undetermined.

Dehydroepiandrosterone (DHEA) is a hormone mainly produced in the adrenal cortex. In addition to its androgenic properties, DHEA has been reported to exert some beneficial effects on obesity, diabetes mellitus, atherosclerosis and ageing (10, 11). We, thus, hypothesized that DHEA may be involved in preventing the development and progression of NAFLD. Recently, however, it has been shown that levels of serum DHEA sulphate (DHEAS), the sulphated congener of DHEA, were rather reduced in patients with histologically diagnosed advanced NASH (12, 13). These observations probably reflect the reduction of DHEA sulphonation, and therefore it is also important to determine serum DHEAS levels in the earlier stage of NAFLD not progressing to

[1]Department of Internal Medicine, Kinki Central Hospital, Japan, [2]Department of Gastroenterology and Hapatology, Kochi Medical School, Japan and [3]Department of Medicine, Nissay Hospital, Japan
Received for publication October 14, 2010; Accepted for publication April 11, 2011
Correspondence to Dr. Masafumi Koga, koga_m@kich.itami.hyogo.jp

Table 1. Clinical Characteristics of the Subjects with or without NAFLD

NAFLD	–	+	p
n	89	69	–
age (years)	51.5 ± 6.9	50.0 ± 7.0	0.197
BMI (kg/m^2)	22.8 ± 2.5	26.6 ± 3.4	<0.001
serum AST (U/L)	19 ± 4	27 ± 13	<0.001
serum ALT (U/L)	20 ± 6	27 ± 13	<0.001
serum triglyceride (mg/dL)	116 ± 53	197 ± 99	<0.001
serum HDL cholesterol (mg/dL)	55 ± 14	48 ± 11	<0.001
serum LDL cholesterol (mg/dL)	125 ± 26	126 ± 25	0.782
fasting plasma glucose (mg/dL)	103 ± 19	109 ± 23	0.082
HOMA-%S (%)	187 ± 80	109 ± 52	<0.001
DHEAS (ng/mL)	1464 ± 661	1814 ± 842	0.004

NASH. The aim of this study was to analyze the clinical significance of DHEAS levels in patients with NAFLD.

Materials and Methods

Subjects

We initially recruited a total of 278 Japanese men who visited the Health Care Center at Kinki Central Hospital for health examinations. Of these subjects we excluded subjects with viral hepatic diseases (positive hepatitis B surface antigen test, positive hepatitis C antibody test and/or past histories of hepatitis B or hepatitis C), diabetes mellitus, renal disease and malignant disease. Subjects who ingested daily alcohol exceeding 20 g/day and subjects who had serum ALT>40 U/L without fatty change of the liver were also excluded. A total of 158 men satisfied the above admission criteria. Their average age was 50.8 ± 7.0 years and body mass index (BMI) was 24.4 ± 3.5 kg/m^2. The institutional committee approved the protocol of this study, and all participants gave their informed consent.

Laboratory methods

Fasting plasma glucose, serum insulin, serum alanine aminotransferase, serum total cholesterol, high density lipoprotein (HDL) cholesterol and serum triglycerides were determined by means of standard laboratory assays. Serum DHEAS was measured by radioimmunoassay (DPC DHEA-S kit, Mitsubishi Kagaku Iatron, Tokyo, Japan). Inter- and intra-assay coefficients of variation in this assay were 12.0% and 4.1% at the concentrations of 600 and 650 ng/mL (14). The homeostasis model assessment insulin sensitivity index (HOMA-%S) was calculated from fasting plasma glucose and serum insulin concentrations by using the correct HOMA evaluation and a computer program (15).

Fatty change of the liver was evaluated by echotomographic examination by assessing hepato-renal contrast, impaired visualization of the hepatic vein borders or the diaphragm (16). When the fatty change was observed in the study patients, they were diagnosed to have NAFLD. Furthermore, we judged the degree of fatty liver as moderate or more when the findings of impaired visualization of the hepatic vein borders or the diaphragm were observed. Otherwise we judged as mild degree of fatty liver.

Statistical analyses

Data are shown as means ± SD. Comparisons of serum DHEAS levels between groups were analyzed with a Student's t-test. Univariate as well as stepwise multivariate regression analyses were performed to assess the effects of variables on serum ALT levels. For the stepwise multivariate regression analyses, the F value for the inclusion of the variables was set at 4.0. In the univariate as well as multivariate regression analyses, serum ALT and serum DHEAS were logarithmically transformed, to correct for skewed distribution. These analyses used a StatView computer program (Version 5.0). The statistical differences were considered to be significant at $p<0.05$.

Results

Of the 158 study subjects, 69 were diagnosed as having NAFLD, whereas the other 89 were not. In the patients with NAFLD BMI, AST, ALT, triglycerides and low density lipoprotein (LDL) cholesterol were significantly higher than in the subjects without it (Table 1). HDL cholesterol and HOMA-%S were significantly lower in the patients with NAFLD than in the subjects without it. Serum DHEAS levels were on average 1,810 ± 840 ng/mL in the patients with NAFLD, which was significantly higher ($p=0.0039$) than those in the subjects without it (1,460 ± 660 ng/mL) (Table 1, Fig. 1A). There was a significant difference between serum DHEAS levels in 29 subjects with a mild degree of fatty liver and in 43 subjects with moderate or more degree of fatty liver (1,890 ± 904 ng/mL vs. 1,769 ± 810 ng/mL; $p=0.5660$). Serum DHEAS levels were not associated with BMI ($R=0.160$, $p=0.0524$) or fasting plasma glucose ($R=-0.022$, $p=0.7819$), while they showed a weak but significant association with body weight ($R=0.155$, $p=0.0443$) and HOMA-%S ($R=-0.180$, $p=0.0216$). Among 69 patients with NAFLD, 19 had elevated ALT levels (>40 U/L). Their serum DHEAS levels were 2,380 ± 950 ng/mL, which were significantly higher ($p<0.0001$) than those in the other 139 subjects with normal ALT levels (≤40 U/L) (1,510 ± 670 ng/mL) (Fig. 1B). They were also significantly higher ($p=0.0003$) than those in 50 NAFLD patients with normal ALT levels (1,600 ± 690 ng/mL). Serum ALT levels were associated positively with serum triglycerides ($R=0.399$, $p<0.0001$), BMI ($R=0.418$, $p<0.0001$), serum DHEAS ($R=0.322$, $p<0.0001$) and fasting plasma glucose ($R=0.183$, $p=0.0204$), and inversely with HOMA-%S ($R=-0.419$, $p<0.0001$), age ($R=-0.224$, $p=0.0043$) and serum HDL cholesterol ($R=-0.186$, $p=0.0183$) in the 160 study subjects (Ta-